Drosophila local search emerges from iterative odometry of consecutive run lengths.

Amir H. Behbahani, Emily H. Palmer, Román A. Corfas, Michael H. Dickinson*
Division of Biology & Bioengineering, California Institute of Technology, Pasadena CA 91125
*author for correspondence

SUMMARY

The ability to keep track of one's location in space is a critical behavior for animals navigating to and from a salient location, but its computational basis remains unknown. Here, we tracked flies in a ring-shaped channel as they executed bouts of search, triggered by optogenetic activation of sugar receptors. Flies centered their back-and-forth local search excursions near fictive food locations by closely matching the length of consecutive runs. We tested a set of agent-based models that incorporate iterative odometry to store and retrieve the distance walked between consecutive events, such as reversals in walking direction. In contrast to memoryless models such as Lévy flight, simulations employing reversal-to-reversal integration recapitulated flies' centered search behavior, even during epochs when the food stimulus was withheld or in experiments with multiple food sites. However, experiments in which flies reinitiated local search after circumnavigating the arena suggest that flies can also integrate azimuthal heading to perform path integration. Together, this work provides a concrete theoretical framework and experimental system to advance investigations of the neural basis of path integration.

KEYWORDS

path integration, odometry, place memory, state-dependent models

INTRODUCTION

For many animals, including humans, the ability to return to a specific location such as a nest or food resource is essential for survival[1]. One strategy for revisiting a specific location is to use external cues such as chemical signals or visual landmarks[2–4]. Another strategy that works in visually poor landscapes or featureless environments[5,6] is to perform path integration, that is, to cumulatively integrate along a path, using a measure of distance traveled (odometry) and body orientation in the direction of travel (heading), thus making it possible to calculate a direct path between any current position and a starting point. Since Darwin first suggested that animals might perform path integration to navigate between food and their nests[7], ample evidence has emerged that many animals employ this strategy. The behavior has been best characterized in ants and bees[8–10], but has been identified in many species including mantis shrimps[11], bats[12], dogs[13] and rats[14]. Whereas the entire process of path integration is difficult to observe directly, it is often manifest in the act of homing, when an animal executes a straight path (a so-called 'home run') back to its nest after completing a tortuous excursion in search of food[15–18]. Animals can also walk directly from their nest to a food site after their first visit to that location[19–21].

Path integration can operate on the scale of hundreds of meters, as exemplified by desert ants[15], or many kilometers, as in bees[8]; however, it can also occur over much smaller spatial scales. In ants, for example, homing is often accompanied by a local search when the forager arrives near the nest, but not near enough to immediately find it[18,22–24]. Although seemingly random, these local searches are structured and centered, suggesting the animal is keeping track of its best estimate of the nest's location. Such local searches are not restricted to central place foragers such as ants and bees; for example, hungry blowflies execute local searches in the vicinity of small food items they have sampled, a behavior that Vincent Dethier described as a 'dance'[25]. *Drosophila melanogaster* also exhibit these local searches near small spots of food[26,27]; and optogenetic activation of sugar receptors substitutes for the presence of actual food in initiating this behavior[27,28]. Fruit flies can perform this food-centered search in the absence of external stimuli or landmarks, indicating that they can rely on idiothetic (internal) information to keep track of their location[27]. These local searches consist of highly tortuous trajectories in which it is difficult to classify instances in which the fly is walking either directly away or toward the food site, making analysis of the behavior quite challenging.

In this study, we deliberately isolated the odometric aspect of path integration by confining flies to an annular channel. In this constrained arena, local searches consist of back-and-forth runs centered around arbitrarily defined food zones where the flies receive optogenetic activation of sugar receptors. By creating several predictive agent-based models, we tested various

hypotheses of the underlying algorithms that flies might use to perform local search. In contrast to simple, memoryless, random search models, algorithms that employed odometric integration recapitulated salient features of the flies' behavior, such as their ability to center search around a food site, even after the food was no longer present. We conclude that one-dimensional local searches in our constrained arena arise from the iterative storage and retrieval of the distance walked during consecutive runs. However, by analyzing cases in which the flies reinitiate local search at a former food location after fully circling the arena, we conclude that flies also keep track of azimuthal heading during local search. Thus, flies may employ multiple integrators when they search for food, a hypothesis that is consistent with observation in ants[8].

RESULTS

Consistent run lengths center local search around a fictive food site

To investigate the behavioral algorithms underlying path integration, we tracked individual flies as they performed local search in an annular arena in which the flies were constrained to walking within a circular channel (Figure 1A). Using an automated closed-loop system, we optogenetically activated sugar-sensing neurons whenever the flies (*Gr5a-GAL4>UAS-CSChrimson*) occupied a designated, featureless, food zone. The 1-second optogenetic light pulse triggered by residence in the food zone was followed by a 15-second refractory period during which time the stimulus was kept off, regardless of the fly's position. Aside from these brief optogenetic pulses, all experiments were conducted in complete darkness. For convenience, we sometimes refer to optogenetic food zones as 'food', and optogenetic activation events as 'food stimuli', although in no cases did the animals experience actual food.

Examples of local searches are plotted in Figures 1B and 1C. To simplify the display and analysis of the data, we transformed the curved trajectories of the flies in the circular channel into one-dimensional paths. All experiments began with a baseline period, during which the optogenetic protocol was not operational. This baseline period was followed by an activation period (AP), during which the optogenetic protocol was in effect, i.e., the fly received the 1-second food stimulus followed by the 15-second refractory period whenever it occupied the food zone. Each AP was followed by a 5-minute post-activation period (post-AP) during which the optogenetic protocol was suspended such that flies did not receive food stimuli. Some experiments consisted of a 40-minute AP, followed by a single 5-minute post-AP (Figure 1B). Other experiments used a repeating trial structure, in which each trial consisted of a 5-minute AP followed by a 5-minute post-AP (Figure 1C).

In the annular arena, flies can either walk clockwise, walk counterclockwise, pause, or perform a reversal to change direction. We defined the distance between two consecutive reversals as a 'run length', *r* (Figure 1B). During the baseline period, flies continuously explored the entire arena, generally performing long runs interspersed with occasional reversals. During the AP, food stimuli consistently triggered local search excursions typically characterized by a stereotyped sequence of behaviors: upon activation of sugar-receptors, the flies briefly paused, continued to walk a few body lengths away from the food, performed a reversal, returned to the food zone, experienced another food stimulus, and then executed a similar excursion in the opposite direction. This process repeated, producing a persistent zig-zagging search pattern during which the flies explored the channel near the food site, while never straying far in either direction. We interpret this behavior to be a simplified one-dimensional version of the two-dimensional local searches that were the subject of recent studies[27,28], as well as those originally identified by Vincent Dethier in the blowfly, *Phormia*[25].

The most informative data regarding whether the flies retain spatial memory of the food site came from the post-AP, when the optogenetic protocol was suspended. Despite no longer receiving food stimuli, flies continued to zig-zag back and forth around the disabled food zone (Figures 1B and 1C, Video S1), suggesting that flies regulate their movement to remain close to the location where they had recently experienced food. We also observed that most flies eventually abandoned their post-AP search after some time (Figures 1B and 1C). To specifically analyze trajectories during which the fly was performing local search, we defined the post-AP as starting at the conclusion of the AP and ending at the onset of what we classified as a 'departure run.' The departure run, which marks the beginning of the post-departure trajectory, was defined as the first run after the conclusion of the AP during which the fly strayed 26 or more body lengths away from the food zone, thus reaching or passing the exact opposite side of the arena from the food zone (Figures 1B and 1C). The total duration of the post-AP trajectory varied—some flies abandoned the food after 1-2 minutes, while others continued searching for the full programed 5 minutes of the post-AP (Figure 1D). Regardless of the duration of the post-AP search, the departure run was usually considerably longer than all the preceding runs (Figures 1D-1F). In other words, rather than slowly expanding or drifting away from the food site, flies typically terminated the post-AP search by performing an exceptionally long run, perhaps reflecting a change in the fly's internal state. This consistent phenomenon motivated our decision to restrict our initial analysis of the post-AP local search behavior to the flies' trajectory prior to the departure run. We will, however, return to interesting features of the flies' behavior after the departure run later in the manuscript.

Despite the absence of food stimuli to provide an iterative landmark, each run during the post-AP search tended to remain centered at the now-disabled food zone (Figures 1G and 1H). To characterize the structure of local search, we further analyzed trajectories on a run-by-run basis. We first examined the distance walked by flies from the point of receiving a food stimulus until their first reversal—a measure we call the 'excursion distance' (Figure 2A). Excursion distances are remarkably consistent; after a food stimulus, flies continue walking approximately 5 body lengths in the same direction they were facing when they arrived at the food (Figure 2B). After walking the excursion distance, flies reverse, return to the food site, and execute another excursion in the opposite direction, thus forming a persistent, zig-zag pattern during the AP (Figure 2A). Food-stimulus-induced excursions are consistent, and so too are run lengths (i.e., the distance between consecutive reversals) during the AP (Figures 2A and 2C). The consistency of run lengths is not simply a consequence of averaging over many flies and many experiments—throughout experiments, the length of each run tends to match that of the preceding run (Figure 2D). During the post-AP, consecutive runs remain highly correlated in length, but tend to increase slightly over the course of the search (Figures 2E-2G). These results are consistent with an odometric hypothesis in which flies store the distance walked during each run and retrieve that information when executing the very next run.

Agent-based models using iterative odometry recapitulate *Drosophila* local search behavior

To test our odometric hypothesis and to investigate the algorithms underlying local search, we constructed different agent-based models of fly behavior. The output of each model—a time series of the fly's position—is generated by a sequence of simulated runs and reversals. First, we tested whether simple models, with run lengths randomly drawn from either an empirically derived dataset or a corresponding Lévy distribution, could recapitulate the flies' behavior during the post-AP. In both of these cases, the models failed to produce a sustained, centered, local search—the simulated flies quickly strayed from the trajectory origin (Figures 3A and 3B). This result suggests that real flies must somehow regulate sequential run lengths during local search.

Based on this initial result, we built two alternative models in which flies are able to perform odometric path integration. In the food-to-reversal integration model (FR), flies integrate the distance walked from the food site to the subsequent reversal (Figure 3C). In the reversal-to-reversal integration model (RR), flies integrate the distance walked between consecutive reversals (Figure 3D). We implemented these models using a state-transition structure. Figures 3E and S1 graphically represents the fly's search algorithm—i.e., how the flies respond to a food

stimulus, at what point they will reverse, and the type of information they can store and retrieve. State-transition diagrams are commonly used in computer science to model systems—self-driving cars, for example[29–31]—where an agent can assume finite states separated by stochastic or deterministic transitions. In these models, flies are initialized in a global search mode, and enter a local search mode when they encounter a food stimulus. When in local search mode, simulated flies use odometry to keep track of their distance walked, and when they have completed their target run length, they perform a reversal and select a new target run length as a function of the prior run length. In contrast to models without odometric integration, simulations using the FR and RR models recapitulated *Drosophila* local search during both the AP and post-AP (Figures 3F and 3G, Video S2). The FR and RR models produce post-AP searches with runs that remain centered near the former food site (Figures 3H and 3I).

Search in the presence of multiple food zones

We next tested whether flies, as well as our state-transition models, can perform local searches around multiple food sites. We modified our annular arena to incorporate two food zones, separated by 9 body lengths along the perimeter of the channel. As expected, flies began searching around the first food site they encountered (Figure 4A). However, on occasions where the fly encountered the second food site during the course of the search, they often expanded their search area to span both food sites (Figure 4A, Video S3). This two-food search continued during the post-AP (Figure 4A, Video S3). The FR and RR models, too, produced stable searches encompassing two food sites, both in the AP and in the post-AP (Figures 4B and 4C, Video S4). When searching around a single food, flies tended to perform reversals on either side of the food (Figure 4D), resulting in the familiar symmetric zig-zag pattern we observed in our earlier experiments with a single food zone. However, after encountering the 2nd food zone, flies tended to not perform reversals during their excursions from one food zone toward the other; instead, they tended to continue walking and reverse only after passing the 2nd food zone (Figure 4D). Both integration models recapitulate this salient feature of search around multiple food sites, supporting the hypothesis that iterative odometric integration underlies *Drosophila* local search (Figures 4E-G). We obtained similar results in experiments in which the food zones were farther apart, separated by 13 body lengths, although flies frequently reverted to single-food search in this configuration (Figure S2). These experiments with a large separation between food zones underscore the salient phenomenon that the flies' inward excursions toward the other food zone were substantially longer than their typical outward excursions—an observation that again

suggests that their behavior involves some sort of odometric memory that allows them to keep track of the location of two food sites.

Flies measure distance walked between consecutive reversals

To test between our two odometric models, we designed an experiment that produces two distinct predictions, depending on whether flies are integrating the distance between a food stimulus and its subsequent reversal (FR model) or between consecutive reversals (RR model). For this paradigm, we modified the arena to feature three food zones, spaced 4.5 body lengths apart (Figure 5A). We modified our optogenetic protocol such that, at the end of the AP, we disabled all but one of the food zones, which remained active for just one single additional visit. The position of this final active food zone (bottom, middle, or top) varied from trial to trial, permitting us to examine how the subsequent run length depended on the location of the final food stimulus (Figure 5B). We found that, regardless of the position of the final food stimulus, flies continue searching across the three food sites during the post-AP (Figures 5C-5E). That is, the first run length of the post-AP (r_1) tends to always match the immediately preceding reversal-to-reversal distance (i.e., the final run length of the AP, r_0) (Figures 5F and 5G, S3), regardless of the position of the last food site they encountered (i.e., the final food-to-reversal distance). These results were highly consistent across two sets of experiments—one collected in March of 2020 and one collected in August and September of 2020 (Figure S4); during the intervening months, our laboratory was shut down due to the COVID-19 pandemic.

Our two integration models make very different predictions for these experiments. In the FR model, because run lengths depend entirely upon the position of food, the final food stimulus sets the target search range for the first post-AP run. Consequently, the FR model produces an abbreviated run length during the post-AP for cases in which the final food stimulus was in either the bottom or middle positions (Figures 5H-5J). That is, in the FR model, the value of r_1 does not necessarily match the value of r_0 but instead varies depending on the position of the final food stimulus (Figures 5K and 5L, S3). In contrast, the RR model produces run lengths that span all three food zones, regardless of the final food stimulus position (Figures 5M-5O); because the RR model stores the distance between consecutive reversals, the value of r_1 always closely matches the value of r_0 (Figures 5P and 5Q, S3), which is what we observed in real flies. Thus, only the RR model recapitulates the behavior of flies in these experiments, supporting the conclusion that flies maintain a centered local search by using iterative odometric integration to specifically keep track of the distance walked between consecutive reversals.

Flies can keep track of their location in two-dimensional space

The circular design of our arena provides us with another opportunity to probe the limits of *Drosophila* spatial memory and navigation. In particular, if flies accurately integrate odometry with their compass heading, then they might be able to recognize that they have returned to the food site after circling the arena—i.e., perform two-dimensional path integration. To test this hypothesis, we conducted experiments in a smaller (~26 body length circumference) circular channel (Figure 6A) to increase the probability that they would walk one or more times around the entire arena. As in some of our earlier experiments (e.g., Figure 1C), we exposed flies to multiple 5-minute APs separated by 5-minute post-APs, in which each pair of APs and post-APs constitutes a trial. To discard the possibility that flies can recognize food sites due to their own chemical signals or other external features, we switched the food zone between two locations, spaced 180^{o} apart, for each AP—i.e., during the 1st trial, the food zone was on the left side of the arena, during the 2nd trial, the food zone was on the right side of the arena, etc. (Figure 6A). Remarkably, after abandoning their local search during the post-AP (i.e., during the post-departure period), many flies reinitiated local search specifically at the former food site, after completing one or more full revolutions around the arena (Figures 6A-6E, Video S5). Flies did not show a preference for searching at other locations of the arena, including the position of the food zone from the immediately preceding trial (Figure 6F). These results suggest that flies are able to integrate odometric and angular heading information to track their location in two-dimensional space.

DISCUSSION

In this study, we developed a novel assay to study the odometric component of path integration in *Drosophila*. We induced local search in a ring-shaped channel by optogenetically stimulating sugar receptors whenever the fly occupied an arbitrarily defined food zone. Local searches in this arena manifested as a persistent zig-zag pattern, in which flies iteratively walked away from and back to the food zone (Figure 1)—a pattern that persisted even after the optogenetic stimulation was no longer provided. We created several agent-based models, and only the ones that incorporated odometric integration recapitulated these local searches (Figure 3). Flies, as well as odometric agent-based models, were able to execute centered searches even in experiments with multiple food sites (Figures 4 and S2). By dynamically manipulating the presentation of multiple food zones in our arena, we were able to explicitly test between two distinct models: one in which flies keep track of the distance traveled from the food site, and another in which they keep track of the distance traveled from one locomotory reversal to the next (Figures 3 and S1).

Both models operate iteratively in that each bout of idiothetic odometry prompts the target distance for the following run. Path integration is typically thought to depend on an animal keeping track of its position relative to a target location, e.g., the location of a nest or a feeding site[8,9]. However, our results more strongly support the reversal-to-reversal (RR) model (Figure 5), suggesting that flies can execute a centered search—in this constrained annular arena—without necessarily keeping track of their distance from a central location. Because our experiments were conducted in the absence of visual or chemical cues, we presume flies measured their translation in the arena via idiothetic self-motion cues such as proprioception or motor efference copy[9]. Whereas the RR model could explain the flies' zig-zagging local search, it could not account for all the behavior we observed; in some cases, flies reinitiated a local search near the original food site after making one or more complete revolutions around the circular channel (Figure 6). Collectively, our results suggest that local search in *Drosophila* likely involves multiple parallel algorithms, one of which relies heavily on odometry, and the other that likely requires input from the compass system as in true path integration.

The success of the RR model in recapitulating this local search is notable because it is substantially simpler than the FR model in its implementation (Figure S1). However, the RR model requires specific assumptions about *Drosophila*'s cognitive abilities, beyond simply odometry, that merit discussion. First, the model requires that the flies are able to recall whether their most recent action is either eating or performing a reversal. Second, when flies encounter a food stimulus, they can compare their current target run length to the current value of their integrator and assess whether the difference between these values is below a preset threshold. This allows flies to recognize whether they have encountered a new food location or whether the center of search has drifted too close to a known food location, in which case they expand their search area accordingly. Last, flies are able to select a target run length after performing their first reversal using a different algorithm than they use after performing later reversals. Future studies investigating the neural basis of path integration may help either uncover circuit mechanisms corresponding to these posited features of our model or reject these predictions.

Although we specifically focused our experiments to study odometry in local search, the circular shape of our arena allowed us to observe whether flies can use azimuthal heading information to perform two-dimensional path integration. We observed that after circling the annular arena, some flies re-initiated local search specifically at the location where they had previously experienced optogenetic stimulation, a behavior that is suggestive of true compass-based path integration[9]. In other words, to accomplish this, flies cannot simply measure the distance walked from the food, but rather must also track their azimuthal heading to recognize

that they have returned to the former food site. It may be that flies simultaneously use multiple integrators, as has been posited in the case of ants[8]. For example, in the annular arena, flies may use the RR model algorithm to perform zig-zagging local search centered at the food; however, simultaneously, flies may be performing two-dimensional path integration to always compute their position relative to the food, which enables them to reinitiate zig-zagging local search after circling the arena. Regardless of how exactly flies are implementing two-dimensional path integration, we conclude that annular arena experiments can be used to execute local search based simply on odometry (i.e., zig-zagging) as well as two-dimensional path integration requiring both odometry and compass-based navigation (i.e., reinitiated local search after circumnavigating the arena).

The obvious locus for the computations associated with our hypotheses is the Central Complex (CX), a set of unpaired nuclei in the core of the insect brain[8,9,32]. Recently, work on CX neuroanatomy[33,34] and physiology[35–37] has characterized a network of neurons that encode compass-heading, leading to models wherein these circuits provide the angular heading information required for path integration. Although mechanisms by which odometric information is encoded and read out by the CX have been proposed[38–41], none have been explicitly tested via genetic or physiological manipulation of behavior.

In sum, we have developed high-throughput assays to quantitatively measure path integration in *Drosophila*, with the ability to specifically isolate the odometric component of path integration. We have also used agent-based modeling to provide a putative computational algorithm for local search. Future studies might employ these assays, in combination with genetic manipulation of neural activity, to test the roles of proprioceptors and compass network neurons in specific aspects of path integration. We anticipate that this work will provide an experimental system and a strong theoretical foundation to further unravel the neural mechanisms of path integration.

METHODS

Animals

We conducted all experiments using 3-to-6-day-old female *Drosophila melanogaster* reared in darkness at 22˚C. We reared the flies on standard cornmeal fly food containing 0.2 mM all trans-Retinal (ATR) (Sigma-Aldrich) and transferred flies 0-2 days after eclosion onto standard cornmeal fly food with 0.4 mM ATR. We supplemented the standard cornmeal food with additional yeast. We obtained the flies by crossing *Gr5a-Gal4* male flies with *UAS-CsChrimson* female virgin flies. Prior to experiments, we wet-starved flies by housing them for 24-40 hours in a vial supplied

with a tissue (KimTech, Kimberly-Clark) containing 1 mL of distilled water with 800µM ATR, and dry-starved flies for up to 150 minutes—including a 45-to-90-minute acclimation period in the experimental arena.

Behavioral experiments with walking flies

We conducted all experiments in a 40 mm-diameter annular arena, except for experiments in Figure 7, where we used a 20 mm-diameter annular arena to increase the likelihood that flies would complete a full revolution during the post-departure period. We constructed the arenas from layers of acrylic with insertable acrylic discs to create the annular channel (4 mm wide and 1.5 mm high). The width of the channel provided sufficient space for flies to walk forward, backward, or turn around at any point in the arena. The channel's low height encouraged the fly to walk either on the floor or the ceiling, rather than the walls of the channel. An upward-directed, custom-made array of 850 nm LEDs, covered by a translucent acrylic panel, was situated 12 cm beneath the arena to provide backlighting for a top-mounted camera (blackfly, FLIR) recording at 30 frames per second. For optogenetic stimulation, we positioned upward directed, 628 nm LEDs (CP41B-RHS, Cree, Inc.) at the center of each food zone, 8.5 mm beneath the arena floor. We covered the chamber lid with a 3 mm thick long-pass acrylic filter (color 3143, ePlastics). The chamber floor was transparent to allow for optogenetic stimulation, and a filter (#3000 Tough Rolux, Rosco Cinegel) was situated beneath the chamber to diffuse the red light used for stimulation, resulting in ~300 W of illumination at the arena floor. The camera, fly chamber, optogenetic lighting panel, and background lighting panel was held within a rigid aluminum frame (80/20) covered with black acrylic to block any external light. We tracked the 2D position of the fly in real time using a python-based machine vision system built on the Robot Operating System (http://florisvb.github.io/multi_tracker). We customized the tracking software to implement closed-loop control of optogenetic stimulation via an LED controller (Arduino Nano) During our initial experiments, we cleaned the behavioral chamber with 100% ethanol after each trial and allowed it to dry before reuse. However, because ethanol causes cracks in the acrylic parts, we stopped using ethanol and instead cleaned the chambers with compressed air. We did not observe any difference in fly behavior between the two cleaning methods (data not shown).

For each experiment, we aspirated a single fly into the behavioral chamber, allowing it to acclimate for 45-90 minutes. The final minutes of this acclimation period correspond to the baseline period in our analyses. Following acclimation, experiments consisted of a specified time-course of activation periods (APs) and post activation-periods (post-APs). During APs, the LED beneath each food zone was turned on for 1 s whenever the centroid of the fly occupied its virtual

perimeter (=2.6 BL). Because optogenetic activation of sugar sensors inhibits locomotion [28], each 1 s pulse was followed by a 15 s refractory period during which the LED remained off, regardless of the fly's position. During the baseline period and post-APs, food zones were not operational such that flies could not receive optogenetic activation. For experiments with multiple APs (as in Figure 1C), each AP and subsequent post-AP was treated as a single trial.

During experiments in Figure 6, we encouraged flies to expand their search to span all three food zones by using an altered protocol during the AP: we disabled each food zone after it was encountered by the fly for the first time; after the fly had encountered all three food zones, all the food zones became operational and remained operational for the remainder of the AP.

For experiments in Figure 7, to discard the possibility that flies were able to find food zones by sensing temperature gradients generated by the LEDs, one of the control zones was outfitted with an LED. When food stimuli were presented, the LEDs at both food zones as well as this control zone were turned on.

For all experiments with a 40-min AP (e.g., Figure 1B), data were discarded if the fly moved less than 10 cumulative body lengths during the first 20 minutes of the AP (N = 3 flies discarded). For all trial-based experiments (e.g., Figure 1C) APs, trials were discarded if the fly moved less than 10 cumulative body lengths during the AP (n = 22 trials discarded).

Agent-based models without odometric integration

The random sampling and Lévy flight models simulated post-AP search by sampling from natural statistics derived from fly search trajectories. For the random sampling model, run lengths were randomly sampled with replacement from the fly post-AP run lengths in Figure 1D (excluding the departure run). For the Lévy flight model, a Lévy distribution was fit to the same data using the function stats.Lévy.fit() from SciPy, and run lengths were drawn randomly from the resulting distribution.

Agent-based models featuring odometric integration

The food-to-reversal (FR) and reversal-to-reversal (RR) integration models are graphically described by the state transition diagrams in Figure S1. The fly is simulated as a point-mass within a simulated environment (Figure S1A) consisting of a linear channel, 52 body lengths (BL) in length. The simulated channel is wrapped at 26 and -26 BL, such that when the fly exits one end of the channel, it enters the other end (i.e., when the fly reaches the -25 BL position, its next step takes it to the 26 BL position, and vice versa). The environment includes one or more food zones (1 BL in length) at specified locations along the linear channel. Similar to our experiments with

real flies, whenever the simulated fly enters a food zone in the simulated environment, it receives a 1 s food stimulus, followed by an 8 s refractory period during which the simulated fly cannot receive a food stimulus; whereas the refractory period is briefer in the simulations than in experiments with real flies, comparisons of temporal aspects of the two systems are somewhat arbitrary because the walking speed of simulated flies is defined artificially. When walking, the fly moves 1 BL per timestep and corresponds to 0.5 s (i.e., the simulated fly walks at 2 BL s^{-1}).

The fly is initialized at the 0 BL position, facing North, and the simulated environment (Figure S1A) is initialized in the food-off state. The fly's integrator (or integrators in the case of the FR model) is initialized with a value of 0, and the fly's target run length value, r_t, is initialized to 0. When the environment is in the food-off state, at each time step, the system checks whether the current time is during the AP, whether the current time is not during a refractory period (i.e., whether the time since the last food stimulus exceeds the duration of the refractory period), and whether the fly occupies a food zone; if all of these conditions are satisfied, the food stimulus is turned on and the environment enters the food-on state. When the environment is in the food-on state, at each time step, if the food stimulus has been on for the duration of the specified stimulus duration (1 timestep), the food stimulus is turned off and the environment returns to the food-off state. The state transition diagram described in Figure S1A—with varying food zone positions, as well as varying baseline, AP, and post-AP durations—is used to simulate the environment in all simulations using the FR and RR models.

Food-to-reversal integration model

In the food-to-reversal (FR) model (Figure S1B), the simulated fly is able to measure walking distance using two integrators—one integrator measuring displacement in the North direction, I_N, and the other integrator measuring displacement in the South direction, I_S. North and South are defined within the simulated fly's reference frame, rather than a global reference frame in the simulated environment. The FR model would not function with a single integrator because the simulated fly must keep track of two distances to accomplish local search during the post-AP in environments with multiple foods: the distance between the foods and the distance walked since the last reversal. Furthermore, the simulated fly is able to store and retrieve its previous action—either a reversal or an eating event. The simulated fly is initialized in the global search mode in the walking state, where it moves forward 1 BL at every time step. When the fly receives a food stimulus, it transitions to the eating state in the local search mode. The fly remains in the local search mode for the remainder of the simulation. While the fly continues to receive the food stimulus, it remains in the eating state. Upon delivery of a food stimulus, the simulation is

advanced 10 timesteps during which the fly remains stationary—this is to mimic the locomotory pause induced by activation of sugar-sensing neurons in *Drosophila*, for the purposes of generating trajectories that resemble *Drosophila* local search.

Upon the termination of the food stimulus in the FR model, the fly selects a new target run length, r_t. If the fly's most recent previous action was a reversal, then r_t is defined to be the sum of the current value of the integrator corresponding to the direction opposite the fly's current walking direction (e.g., if the fly's current walking direction is North, the relevant integrator is the South integrator) and a value drawn from the distribution of run lengths induced by a food stimulus, C_f (analogous to the distribution of fly excursion distances in Figure 2B), and subsequently both integrators are set to zero; this course of action represents the fly responding to having received its first food stimulus since performing a reversal. On the other hand, if the fly's most recent previous action was an eating event and the difference between the current target run length and the value of whichever integrator is highest is below 1 BL, then the new target run length, r_t, is defined to be the sum of the value of whichever integrator is highest and a value drawn from C_f; this course of action represents the simulated fly interpreting the food stimulus as a new food location and extending its run length to expand its local search to encompass the new food in addition to the prior food(s). Finally, if neither condition holds, the fly does not select a new target run length.

Having responded to the food stimulus, the simulated fly sets its previous action to an eating event and transitions to a walking state. At each time step while in the walking state, the fly moves forward 1 BL, and the integrators are incremented accordingly—i.e., if the walking direction is North, the North integrator is increased by one and the South integrator is decreased by one (with a minimum value of zero), and vice versa. The fly continues walking until the integrator corresponding to the direction of motion equals or exceeds r_t. At this point, a new target run length, r_t, is selected based on the fly's previous action. If the previous action was an eating event, r_t is defined to be the sum of the value of whichever integrator is highest, and a value drawn from C_f; this ensures that the search stays centered over the food zone(s). On the other hand, if the previous action was a reversal, r_t is defined to be the sum of the value of whichever integrator is highest, and a value drawn from C_Δ—the distribution of the differences in lengths between consecutive runs (analogous to the distribution in Figure 2D). After the selection of a new target run length, walking direction is switched (i.e., if the current direction is North, it becomes South and vice versa). The fly remains in the walking state and returns to the eating state if it receives a food stimulus.

Reversal-to-reversal integration model

In the reversal-to-reversal (RR) model (Figure S1C), the simulated fly is able to measure walking distance using an integrator, I. Furthermore, the simulated fly is able to store and retrieve its previous action—either a reversal or an eating event. As in the FR model, the fly is initialized in the global search mode in the walking state and transitions to the local search mode eating state upon receiving a food stimulus. The fly remains in the local search mode for the remainder of the simulation. The fly stays in the eating state until the termination of the food stimulus, at which time it transitions to the walking state. If the difference between the fly's current target run length and the integrator value is below 3 BL, a new target run length, r_t, is defined to be the sum of the current integrator value and a value drawn from the distribution of run lengths induced by a food stimulus, C_f (analogous to the distribution of fly excursion distances in Figure 2B); this course of action represents the simulated fly interpreting the food stimulus as a new food location, and extending its run length to expand its local search to encompass the new food in addition to the prior food(s). Otherwise, a new target run length is not selected. Because this algorithm also ensures that the fly never reverses within 3 BL of a food zone, it can re-center the search at the food location(s); unlike the FR model, the RR model search is not iteratively re-centered at every food stimulus, and thus would drift more rapidly than the FR model, even during the AP, were it not for this feature.

Having responded to the food stimulus, the simulated fly sets its previous action to an eating event and transitions to the walking state. While walking, the integrator increases by one at each time step as the fly moves forward 1 BL. When the integrated value exceeds the target run length, the integrator is set to zero and the fly performs a reversal. In the RR model, the fly is able to distinguish its first reversal from all subsequent reversals during the simulated experiment. If it is indeed the first reversal of the experiment, the new target run length is defined to be the sum of the current target run length and a value drawn from C_f; this ensures that the search stays centered over the food zone(s). On the other hand, if it is not the first reversal of the sequence, and the fly's most recent previous action was an eating event, the new target run length is defined to be the sum of the previous target run length and a value drawn from $C_{\Delta,AP}$—the distribution of the difference in length between consecutive runs during the AP. Otherwise, the new target run length is defined to be the sum of the previous target run length and a value drawn from $C_{\Delta,post\text{-}AP}$—the distribution of the difference in length between consecutive runs during the post-AP. Regardless of how the new target run length is selected, the simulated fly sets its previous action

to a reversal and returns to the walking state. The fly remains in the walking state and returns to the eating state if it receives a food stimulus.

Run length distributions for odometric integration models

In both the FR and RR models, the simulated fly selects a new target run length following a food stimulus by sampling from the food-induced run length distribution $C_f \sim \mathcal{N}(\mu_f, \sigma_f)$. To select a new target run length following a reversal, the FR model samples from $C_\Delta \sim \mathcal{N}(\mu_\Delta, \sigma_\Delta)$—the distribution of the difference in length between consecutive runs—whereas the RR model samples from $C_{\Delta,\mathrm{AP}} \sim \mathcal{N}(\mu_{\Delta,\mathrm{AP}}, \sigma_{\Delta,\mathrm{AP}})$ or $C_{\Delta,\mathrm{post-AP}} \sim \mathcal{N}(\mu_{\Delta,\mathrm{post-AP}}, \sigma_{\Delta,\mathrm{post-AP}})$, depending on whether the most recent action was an eating event ($C_{\Delta,\mathrm{AP}}$) or a reversal ($C_{\Delta,\mathrm{post-AP}}$). Whereas the sampled distributions are analogous to the observable statistics of *Drosophila* local search, they cannot be derived from fly data, because we cannot directly measure target run length in a real fly. For example, when a fly encounters a new food location and continues walking several body lengths before performing a reversal, the resulting total run length may be the sum of the original target run length (selected prior to encountering the new food) and an additional run length induced by the new food stimulus; we cannot determine the true value of either component of the fly's algorithm. Thus, the distributions from fly data cannot be directly implemented in the model. Instead, we determined the distribution parameters by performing a grid search over the parameter space to minimize a cost function (Equation 1). At each point in the grid search, the model was run 250 times. The cost function was designed to minimize the differences between the statistics of *Drosophila* local search and those of the given model. Given N parameters we sought to match between the data and simulations, we fit an appropriate distribution (e.g., normal or gamma) to the i^{th} parameter to get the distribution $p_i \sim X_i\left(x_{i,1}, x_{i,2}, \ldots, x_{i,M_i}\right)$, such that the distribution is governed by M_i values. We fit the distribution to both the data and the simulations, yielding $p_i^d \sim X_i\left(x_{i,1}^d, x_{i,2}^d, \ldots, x_{i,M_i}^d\right)$ for the data and $p_i^s \sim X_i\left(x_{i,1}^s, x_{i,2}^s, \ldots, x_{i,M_i}^s\right)$ for the simulations (where d and s denote 'desired' and 'simulated', respectively). We then calculated the total cost across all parameters, normalizing for the number of values governing each distribution:

$$\mathrm{Cost} = \sum_{i=1}^{N} \frac{1}{M_i} \sum_{j=1}^{M_i} \left(\frac{x_j^s}{x_j^d} - 1 \right)^2 \qquad (1)$$

The relevant parameters we sought to match between the data and simulations were the excursion distances ($D_O^d \sim \Gamma(\alpha = 2.81, \mathrm{loc} = 0.22, \mathrm{scale} = 1.88)$), the difference in length between

consecutive runs ($\Delta r^d_{N,\mathrm{AP}} \sim \mathcal{N}(\mu = 0.09, \sigma = 4.91)$, $\Delta r^d_{N,\mathrm{post-AP}} \sim \mathcal{N}(\mu = 0.71, \sigma = 6.84)$), and the locations of run midpoints ($M^d_{\mathrm{ap}} \sim \Gamma(\alpha = 1.06, \mathrm{loc} = -5.11 * 10^{-6}, \mathrm{scale} = 0.16)$, $M^d_{\mathrm{post-AP}} \sim \Gamma(\alpha = 0.55, \mathrm{loc} = 7.60 * 10^{-5}, \mathrm{scale} = 1.33)$. These values were derived using SciPy's stats.gamma.fit() and stats.norm.fit() functions. The distributions used in the FR model were $C_f \sim \mathcal{N}(\mu_f = 3.5, \sigma_f = 3.7)$ and $C_\Delta \sim \mathcal{N}(\mu_\Delta = 0.25, \sigma_\Delta = 1.75)$. The distributions used in the RR model were $C_f \sim \mathcal{N}(\mu_f = 3.56, \sigma_f = 2.31)$, $C_{\Delta,\mathrm{AP}} \sim \mathcal{N}(\mu_{\Delta,\mathrm{AP}} = -0.25, \sigma_{\Delta,\mathrm{AP}} = 1.56)$ and $C_{\Delta,\mathrm{post-AP}} \sim \mathcal{N}(\mu_{\Delta,\mathrm{post-AP}} = 1.25, \sigma_{\Delta,\mathrm{post-AP}} = 1.06)$. The final cost for the FR model was ~21 and the final cost for the RR model was ~28.

Behavioral analysis of walking flies

The dataset for each experiment consisted of an array of X and Y coordinates representing the 2D positions of the fly, as well as an array of LED states (on or off) for each food zone. Data were sampled at ~30 Hz. We converted the positional coordinate of the fly to an angular position in the ring-shaped arena, and treated the fly as a point mass along the circumference of the arena. The beginning of each AP was defined as the first food stimulus, and the end of each AP (and the beginning of the subsequent post-AP) was defined as the final food stimulus. To process data, we discarded occasional frames where the fly was either not tracked, where a second object was tracked in addition to the fly (e.g., fly poop), or where the tracked position jumped more than 3 mm within two consecutive frames (e.g., due to sporadic tracking of another object). Because the position of food zones varied slightly due to variations in the fabrication and assembly of arenas, we defined the center of each food zone for each experiment as the midpoint between the extrema of fly locations at food stimulus events associated with the food zone.

Data reporting and statistical analysis

We generated all figures using the python library matplotlib. Throughout the paper, we calculated the 95% confidence intervals using built-in SciPy statistical functions to compute the standard error of the mean and the Student's t-distribution. For the statistical significance analysis, we used distributions of mean values generated by 2000 bootstrap iterations. For datasets with overlapping discretized ranges, we plotted datapoints in a random order for presentation purposes.

ACKNOWLEDGMENTS

We would like to thank all member our lab for helpful discussions. Will Dickson provided essential help with programming and construction of our experimental set-up. Research reported in this publication was supported by the National Institute of Neurological Disorders and Stroke of the National Institutes of Health under Award U19NS104655.

AUTHOR CONTRIBUTIONS

AB conducted all experiments, under the supervision of MD. EP developed the state-based models of behavior. AB, RAC and EP analyzed data and prepared all figures. AB, RAC, EP and MD wrote the paper.

DECLARATION OF INTERESTS

We have no competing interest to declare.

FIGURE LEGENDS

Figure 1. Repeated back-and-forth excursions constitute a local search around a fictive food location.

(A) Schematic of the experimental setup (left) and annular arena (right). An overhead camera tracks the position of an individual *Gr5a-GAL4>UAS-CsChrimson* female fly, in real-time, as it explores a 4 mm-wide circular channel, ~52 body lengths (BL) in circumference. Whenever the fly occupies the featureless food zone, it receives a one-second pulse of optogenetic activation of sugar-sensing neurons via a 628 nm LED positioned beneath the channel, followed by a 15-second refractory period during which the fly cannot receive activation. An infrared (IR) backlight and IR-transmitting lid enable behavioral tracking while otherwise maintaining complete darkness for the fly aside from the brief optogenetic pulses. (B) Example fly trajectory. To simplify the display and analysis of the data, we transformed the curved trajectories of the flies in the circular channel into a wrapped one-dimensional path. This experiment begins with a baseline period, during which the fly does not receive optogenetic activation, followed by a 40-minute activation period (AP, red) during which the optogenetic protocol is operational, followed by a post-activation-period (post-AP, blue) during which the optogenetic protocol is switched off. The post-AP is defined as ending when the fly executes its first run straying more than 26 body lengths (i.e., ½ the arena perimeter) from the food zone, hereafter termed the ‘departure run’. The

remaining trajectory is referred to as post-departure (grey). Optogenetic stimulation events during the AP are indicated as tick-marks (top). Inset: trajectories are analyzed to classify reversals of walking direction and run lengths (*r*)., i.e., the distance between consecutive reversals. (C) As in (B), for an experiment with six serial trials each consisting of a 5-minute AP followed by a 5-minute post-AP. (D) Sequences of post-AP runs, and their associated departure run, sorted by the duration of the post-AP. Each row corresponds to a single trial from experiments as in (C), where the length of each box corresponds to the duration of each run, and the color of each box indicates run length. (N = 22 flies, n = 110 trials). Note that in 11 trails at the bottom of the panel, the flies did not execute a departure run before the next AP began. (E) Run lengths for the final 10 runs of the post-AP, as well as the departure run, from data in (D). Data from trials with fewer than 10 post-AP runs are included. Throughout the paper, circles depict means, error bars depict 95% confidence intervals, and violin plots indicate full data distributions. (F) Length comparison of the longest post-AP run, and corresponding departure run, for each trial, from data in (D). The 11 trials without a departure run were not included in this analysis. (G) Distribution of the absolute value of the midpoint position of all runs from all trials from experiments as in (C), during baseline, AP, and post-AP. The 0 position indicates the center of the food zone. (N = 22 flies, n = 110 trials). Note, that because the data are expressed as absolute values, negative values are not permitted. (H) As in (G), showing the absolute value of the mean midpoint position of all runs from each fly. Grand means are plotted alongside individual datapoints.

Figure 2. Local searches feature consistent run lengths.

(A) Schematic, showing features of local search. After encountering a food stimulus during the AP, flies walk a given excursion distance (grey), reverse direction, and perform a run back towards the food. The distance between two consecutive reversals is a run length (*r*), where r_0 is the run length between the final reversal of the AP and the first reversal of the post-AP. (B) Mean distribution of excursion distances, from the 40-min AP experiments as in Figure 1B. (N = 29 flies). (C) Run lengths for the final 16 runs of the AP, including r_0, from the 40-min AP experiments. Data from trials with fewer than 16 AP runs are included. (N = 29 flies). (D) Mean distribution of the difference in length between consecutive runs (Δr) during the AP, the 40-min AP experiments. (N = 29 flies). (E) Run lengths for the final 6 runs of the AP, including r_0, and the first 10 runs of the post-AP, from the trial-based experiments as in Figure 1C. (N = 22 flies, n = 110 trials). Labels indicate the final run of the AP (r_0) and the first run of the post-AP (r_1). (F) Relationship between the final run of the AP (r_0) and the first run of the post-AP (r_1) from data in (E). Black dots indicate r_0 vs. r_1 for 6 trials from the fly in Figure 1C, and the black line indicates the linear regression for

this fly. Grey lines indicate linear regressions for all remaining flies with data from at least 3 trials. (N = 20 flies). (G) Mean distribution of the difference in length between consecutive runs (Δr) during the first 10 runs of the post-AP, from data in (E).

Figure 3. Agent-based models using iterative odometric integration recapitulate *Drosophila* local search.

(A) Six representative example trajectories from simulations for which run lengths were randomly drawn from the distribution of run lengths in Figure 1D (excluding the departure runs). Trajectories begin at the 0 position and are terminated when the simulated fly reaches 26 body lengths from the point of origin. (B) As in (A) from simulations for which run lengths were drawn from a Lévy flight distribution fit to the distribution of run lengths in Figure 1D (excluding the departure runs). (C) Schematic of food-to-reversal (FR) integration model. The fly keeps track of the distance walked between the location of a food stimulus and the subsequent reversal. This integrated distance influences the choice of target run length (r_t) for the following run.

(D) Schematic of reversal-to-reversal (RR) integration model. The fly keeps track of the distance walked between consecutive reversals. This integrated distance influences the choice of target run length (r_t) for the following run. (E) Schematic of the state-transition diagram for FR and RR integration models. Arrows indicate transitions—governed by conditions—between search modes, behavioral states, and computational processes. For detailed state transition diagrams describing the FR and RR models, as well as the simulated environment, see Figure S1. (F) Example trajectory of FR model simulation, showing baseline, AP, and post-AP. Plotting conventions as in Figure 1B. (G) As in (F) for a RR model simulation. (H) Distribution of absolute value of mean post-AP midpoint position of all runs for agent-based models (n = 300 simulations as in (F) and (G)). For comparison, fly data are replotted from Figure 1H. (I) Statistical comparison of agent-based models and fly data. Histograms show distributions of the absolute value of mean run midpoint position, calculated from 2,000 random samples from distributions in (H). Vertical lines indicate the grand mean run midpoint of fly data in (H).

Figure 4. Iterative odometric integration enables local search around multiple fictive food sites.

(A) Example trajectory of a fly exploring an annular arena with two food zones, spaced 9 body lengths (BL) apart. The experiment consists of a baseline period, AP, and post-AP. Plotting conventions as in Figure 1B. (B) As in (A), for a simulation using the FR model. (C) As in (A), for a simulation using the RR model. (D) Mean distribution of reversal locations during fly experiments

as in (A). Histograms were calculated using 2 BL bins. Distributions are plotted for the one-food search (1F, light red), the two-food search (trajectory after the fly has encountered the 2nd food zone, 2F, dark red), and the post-AP (blue). To align data for analysis, distributions from some experiments were inverted such that the location of the 1st food zone is always at the -4.5 BL position. For each experiment, 1F, 2F, or post-AP distributions consisting of fewer than 5 total reversals were discarded from this analysis. (N = 29 flies). (E) As in (D) for simulations using the FR model. (F) As in (D) for simulations using the RR model. (G) Distribution of absolute value of mean midpoint position of all runs for odometric integration models (n = 300 simulations), as well as from each fly, from data in (D-F). Grand mean of the absolute value of run midpoint positions is plotted alongside fly data. (H) Statistical comparisons of run midpoints of odometric integration models and fly data during experiments with multiple food zones. Histograms show the distribution of the absolute value of mean run midpoint position for the indicated dataset and experimental period, calculated from 2,000 random samples from distributions in (G). Vertical lines indicate mean or grand mean of indicated dataset or experimental period from data in (G).

Figure 5. Flies center local search around multiple fictive food sites by integrating the distance walked between consecutive reversals.

(A) Schematic of the annular arena with three food zones, spaced 4.5 body lengths apart.

(B) Schematic of the experimental paradigm. At the conclusion of the AP, two of the food zones were disabled while one food zone remained capable of providing an additional single optogenetic pulse. For each trial, the final operational food zone was designated to be either the bottom, middle, or top. For trials where the final 3 or more runs during the AP spanned all three food zones, we compared r_0 and r_1, where r_0 is the run length between the final reversal of the AP and the first reversal following the final food stimulus. (C-E) Example trajectories of a fly searching across three food zones, in which the final food stimulus is in either the bottom (C), middle (D), or top (E) position. (F) Relationship between r_0 and r_1 for three-food experiments with flies, in which the final food stimulus is in either the bottom, middle, or top position. Lines and r^2 values indicate linear regressions for the three conditions. (N = 45 flies, n = 166 trials). (G) Statistical comparisons of run lengths in three-food experiments where the final food stimulus is in either the bottom, middle, or top position. Histograms show distributions of the mean difference between r_1 and r_0, calculated from 2,000 random samples of the mean of 10 points from distributions in (F). (H-L) As in (C-G), for simulations using the FR model. (n = 300 simulations). (M-Q) As in (C-G), for simulations using the RR model. (n = 300 simulations).

Figure 6. Flies reinitiate a local search at a former fictive food site after circling the arena.
(A) Schematic of the smaller annular arena (~26 body lengths), indicating the location of the food zone for each trial, as well as control zones used for analysis. Experiments were done as in Figure 1C, but each food zone was 1.3 body lengths, and the food zone location was alternated from trial to trial. (B) Example post-AP (grey) and post-departure (colored) trajectories from a single experiment where each line corresponds to a single trial and shows the unwrapped trajectory, with gridlines indicating full revolutions around the arena. To align data for analysis, trajectories from even-numbered trials were shifted such that the location of the food zone is always at 0.
(C) Mean distribution of fly transits for post-departure trajectories in (B). Transits were calculated using bins 2 BL wide and counted when a fly entered a bin from one side and exited the bin from the other side. (D) Heatmap indicating distribution of transits during post-departure trajectories, calculated using 4 bins per revolution (dividing the arena into quadrants centered on the food zone, disabled food zone, and control zones). Each column represents a single trial, with columns sorted by frequency of transits at the 1 or -1 revolution position. (N = 28 flies, n = 168 trials).
(E) Mean transit distribution for data in (D). Shaded grey region indicates 95% confidence interval.
(F) Number of run midpoints in each arena quadrant during post-departure trajectories. Each line shows the mean values for a single fly, where data from both control quadrants were averaged together.

SUPPLEMENTAL INFORMATION

Supplementary Figure 1. State-transition diagrams describing agent-based odometric integration models of *Drosophila* local search, related to Figure 3

(A) Left: Schematic of the simulated 1-dimensional environment. The example shown here is for a simulated environment with a single food zone. Right: State transition diagram for the simulated environment. The simulated environment is in either the food on or off state. Transitions between these states, via processes, are determined by the conditions at each timestep of the simulation. See methods for details. (B-C) State transition diagrams for the food-to-reversal (FR) integration model (B) and the reversal-to-reversal (RR) integration model (C). The simulated fly can either be in an eating or walking state, within either a global or local search mode. Transitions between these states and modes, sometimes via processes, are determined by the conditions at each timestep of the simulation. (r_t = target run length, BL = body lengths, I = Integrator, N = North, S = South, prevAction = previous action, firstRev = first reversal). The variables C_f, C_Δ, $C_{\Delta,AP}$, and $C_{\Delta,post\text{-}AP}$, represent a value drawn from the corresponding distribution. See methods for details.

Supplementary Figure 2. Iterative odometric integration enables local search around fictive food sites spaced 13 body lengths apart, related to Figure 4

(A-I) As in Figure 4, for experiments where the food zones are located 13 body lengths apart. (N = 27 flies).

Supplementary Figure 3. Flies and odometric integration models maintain constant run lengths during the AP, related to Figure 6

(A) Schematic of the annular arena with three food zones, spaced 4.5 BL apart. (B) Schematic of experimental conditions. At the conclusion of the AP, two of the food zones were disabled, while one food zone remained temporarily operational, capable of providing an additional single optogenetic pulse. For each trial, the final operational food zone was randomly designated to be either the bottom, middle, or top food zone. For trials where at least the final 3 or more runs during the AP spanned all three food zones, we analyzed the distance between the final two reversals during the AP (r_0) as well as the distance between the penultimate reversal of the AP and the preceding reversal (r_{-1}). (C) Relationship between r_0 and r_{-1} for three-food experiments with flies, where the final food stimulus is in either the bottom, middle, or top position. Lines and r^2 values indicate linear regressions for the three conditions. (N = 45 flies, n = 166 trials).

(D) Statistical comparisons of run lengths in three-food experiments where the final food stimulus is in either the bottom, middle, or top position. Histograms show distributions of the mean difference between r_{-1} and r_0, calculated from the means of 2000 random samples of 10 points from the distributions in (C). (E-F) As in (C-D), for simulations using the FR model. (n = 300 simulations per condition). (G-H) As in (C-D), for simulations using the RR model. (n = 300 simulations per condition).

Supplementary Figure 4. Results from 3-food paradigm were highly consistent across experiments performed many months apart, related to Figure 6

(A) Relationship between r_0 and r_1 for three-food experiments conducted in March 2020 (dataset 1, green, N = 23 flies, n = 78 trials) or September 2020 (dataset 2, purple, N = 22 flies, n = 88 trials), for trials where the final food stimulus is in the bottom position. Lines and r^2 values indicate linear regressions for the two datasets. These datasets are combined in Figure 6. (B) Statistical comparisons of three-food experiment datasets. Histograms show distributions of the mean difference between r_1 and r_0, calculated from the means of 2000 random samples of 10 points from the distributions in (A). (C-D) As in (A-B), for trials where the final food stimulus is in the middle position. (E- F) As in (A-B), for trials where the final food stimulus is in the top position.

Video S1. **Animations of *Drosophila* local search behavior, related to Figure 1**

Each animation depicts fly position (black circle) during one trial from the experiment plotted in Figure 1C. A motion trail depicts fly position during the previous 5 seconds. Optogenetic activation events are indicated by a red circle to the left of the food zone. The total elapsed time and experimental period are indicated. Playback is at 8x speed.

Video S2. Animations of simulated data from odometric integration models of local search, related to Figure 3

Left: food-to-reversal model simulation, from the experiment plotted in Figure 3F. Right: reversal-to-reversal model simulation, from the experiment plotted in Figure 3G. A motion trail depicts fly position during the previous 10 seconds. Plotting conventions as in Video S1. Playback is at 8x speed.

Video S3. Animation of *Drosophila* local search around two food zones, related to Figure 4

The animation depicts fly position during the experiment plotted in Figure 4A. The animation begins shortly before the fly has encountered the 2nd food zone. A motion trail depicts fly position during the previous 12 seconds. Plotting conventions as in Video S1. Playback is at 20x speed.

Video S4. Animations of simulated data from odometric integration models of local search around two food zones, related to Figure 4

Left: food-to-reversal model simulation, from the experiment plotted in Figure 4B. Right: reversal-to-reversal model simulation, from the experiment plotted in Figure 4C. A motion trail depicts fly position during the previous 10 seconds. Plotting conventions as in Video S1. Playback is at 20x speed.

Video S5. Animations of *Drosophila* local search behavior in a small annular arena, related to Figure 7

Each animation depicts fly position during one trial from the experiment plotted in Figure 7B. A motion trail depicts fly position during the previous 5 seconds. Plotting conventions as in Video S1. Playback is at 8x speed.

REFERENCES

1. Pyke, G.H. (1984). Optimal foraging theory. Annu. Rev. Ecol. Syst. *15*, 523–575.

2. Whishaw, I.Q., and Brooks, B.L. (1999). Calibrating space: exploration is important for allothetic and idiothetic navigation. Hippocampus *9*, 659–667.

3. Wolf, H. (2011). Odometry and insect navigation. J. Exp. Biol. *214*, 1629–1641.

4. Wehner, R., and Müller, M. (2006). The significance of direct sunlight and polarized skylight in the ant's celestial system of navigation. Proc. Natl. Acad. Sci. *103*, 12575–12579.

5. Bühlmann, C., Cheng, K., and Wehner, R. (2011). Vector-based and landmark-guided navigation in desert ants inhabiting landmark-free and landmark-rich environments. J. Exp. Biol. *214*, 2845–2853.

6. Merkle, T., Knaden, M., and Wehner, R. (2006). Uncertainty about nest position influences systematic search strategies in desert ants. J. Exp. Biol. *209*, 3545–3549.

7. Darwin, C. (1873). Origin of Certain Instincts. Nature *7*, 417–418.

8. Collett, T.S. (2019). Path integration: how details of the honeybee waggle dance and the foraging strategies of desert ants might help in understanding its mechanisms. J. Exp. Biol. *222*.

9. Heinze, S., Narendra, A., and Cheung, A. (2018). Principles of insect path integration. Curr. Biol. *28*, R1043–R1058.

10. Ronacher, B. (2008). Path integration as the basic navigation mechanism of the desert ant Cataglyphis fortis (Forel, 1902)(Hymenoptera: Formicidae). Myrmecol. News *11*, 53–62.

11. Patel, R.N., and Cronin, T.W. (2020). Mantis Shrimp Navigate Home Using Celestial and Idiothetic Path Integration. Curr. Biol. *30*, 1981-1987.e3.

12. Aharon, G., Sadot, M., and Yovel, Y. (2017). Bats Use Path Integration Rather Than Acoustic Flow to Assess Flight Distance along Flyways. Curr. Biol. *27*, 3650-3657.e3.

13. Seguinot, V., Cattet, J., and Benhamou, S. (1998). Path integration in dogs. Anim. Behav. *55*, 787–797.

14. Whishaw, I.Q. (1998). Place Learning in Hippocampal Rats and the Path Integration Hypothesis. Neurosci. Biobehav. Rev. *22*, 209–220.

15. Müller, M., and Wehner, R. (1988). Path integration in desert ants, Cataglyphis fortis. Proc. Natl. Acad. Sci. *85*, 5287–5290.

16. Turner, C.H. (1907). The homing of ants: an experimental study of ant behavior (University of Chicago.).

17. Wehner, R., and Srinivasan, M.V. (1981). Searching behaviour of desert ants, genusCataglyphis (Formicidae, Hymenoptera). J. Comp. Physiol. *142*, 315–338.

18. Wittlinger, M., Wehner, R., and Wolf, H. (2006). The ant odometer: stepping on stilts and stumps. science *312*, 1965–1967.

19. Collett, M., Collett, T.S., and Wehner, R. (1999). Calibration of vector navigation in desert ants. Curr. Biol. *9*, 1031–S1.

20. Schmid-Hempel, P. (1984). Individually different foraging methods in the desert ant Cataglyphis bicolor (Hymenoptera, Formicidae). Behav. Ecol. Sociobiol. *14*, 263–271.

21. Wolf, H., and Wehner, R. (2000). Pinpointing food sources: olfactory and anemotactic orientation in desert ants, Cataglyphis fortis. J. Exp. Biol. *203*, 857–868.

22. Collett, M., and Collett, T.S. (2000). How do insects use path integration for their navigation? Biol. Cybern. *83*, 245–259.

23. Wehner, R., and Wehner, S. (1986). Path integration in desert ants. Approaching a long-standing puzzle in insect navigation. Monit. Zool. Ital.-Ital. J. Zool. *20*, 309–331.

24. Wittlinger, M., Wehner, R., and Wolf, H. (2007). The desert ant odometer: a stride integrator that accounts for stride length and walking speed. J. Exp. Biol. *210*, 198–207.

25. Dethier, V. (1957). Communication by insects: physiology of dancing. Science *125*, 331–336.

26. Bell, W.J., Cathy, T., Roggero, R.J., Kipp, L.R., and Tobin, T.R. (1985). Sucrose-stimulated searching behaviour of Drosophila melanogaster in a uniform habitat: modulation by period of deprivation. Anim. Behav. *33*, 436–448.

27. Kim, I.S., and Dickinson, M.H. (2017). Idiothetic path integration in the fruit fly Drosophila melanogaster. Curr. Biol. *27*, 2227–2238.

28. Corfas, R.A., Sharma, T., and Dickinson, M.H. (2019). Diverse food-sensing neurons trigger idiothetic local search in Drosophila. Curr. Biol. *29*, 1660–1668.

29. Guidolini, R., Scart, L.G., Jesus, L.F., Cardoso, V.B., Badue, C., and Oliveira-Santos, T. (2018). Handling pedestrians in crosswalks using deep neural networks in the IARA autonomous car. In 2018 International Joint Conference on Neural Networks (IJCNN) (IEEE), pp. 1–8.

30. Possatti, L.C., Guidolini, R., Cardoso, V.B., Berriel, R.F., Paixão, T.M., Badue, C., De Souza, A.F., and Oliveira-Santos, T. (2019). Traffic light recognition using deep learning and prior maps for autonomous cars. In 2019 International Joint Conference on Neural Networks (IJCNN) (IEEE), pp. 1–8.

31. Badue, C., Guidolini, R., Carneiro, R.V., Azevedo, P., Cardoso, V.B., Forechi, A., Jesus, L., Berriel, R., Paixão, T.M., Mutz, F., et al. (2020). Self-driving cars: A survey. Expert Syst. Appl., 113816.

32. Stone, T., Webb, B., Adden, A., Weddig, N.B., Honkanen, A., Templin, R., Wcislo, W., Scimeca, L., Warrant, E., and Heinze, S. (2017). An anatomically constrained model for path integration in the bee brain. Curr. Biol. *27*, 3069–3085.

33. Franconville, R., Beron, C., and Jayaraman, V. (2018). Building a functional connectome of the Drosophila central complex. eLife *7*, e37017.

34. Hulse, B.K., Haberkern, H., Franconville, R., Turner-Evans, D.B., Takemura, S., Wolff, T., Noorman, M., Dreher, M., Dan, C., Parekh, R., et al. (2020). A connectome of the Drosophila central complex reveals network motifs suitable for flexible navigation and context-dependent action selection. bioRxiv, 2020.12.08.413955.

35. Green, J., Adachi, A., Shah, K.K., Hirokawa, J.D., Magani, P.S., and Maimon, G. (2017). A neural circuit architecture for angular integration in Drosophila. Nature *546*, 101–106.

36. Kim, S.S., Rouault, H., Druckmann, S., and Jayaraman, V. (2017). Ring attractor dynamics in the Drosophila central brain. Science *356*, 849–853.

37. Turner-Evans, D., Wegener, S., Rouault, H., Franconville, R., Wolff, T., Seelig, J.D., Druckmann, S., and Jayaraman, V. (2017). Angular velocity integration in a fly heading circuit. eLife *6*, e23496.

38. Adden, A., Stewart, T.C., Webb, B., and Heinze, S. (2020). A neural model for insect steering applied to olfaction and path integration. bioRxiv, 2020.08.25.266247.

39. Stone, T., Webb, B., Adden, A., Weddig, N.B., Honkanen, A., Templin, R., Wcislo, W., Scimeca, L., Warrant, E., and Heinze, S. (2017). An anatomically constrained model for path integration in the bee brain. Curr. Biol. *27*, 3069–3085.

40. Lu, J., Westeinde, E.A., Hamburg, L., Dawson, P.M., Lyu, C., Maimon, G., Druckmann, S., and Wilson, R.I. (2020). Transforming representations of movement from body- to world-centric space. bioRxiv, 2020.12.22.424001.

41. Lyu, C., Abbott, L.F., and Maimon, G. (2020). A neuronal circuit for vector computation builds an allocentric traveling-direction signal in the Drosophila fan-shaped body. bioRxiv, 2020.12.22.423967.

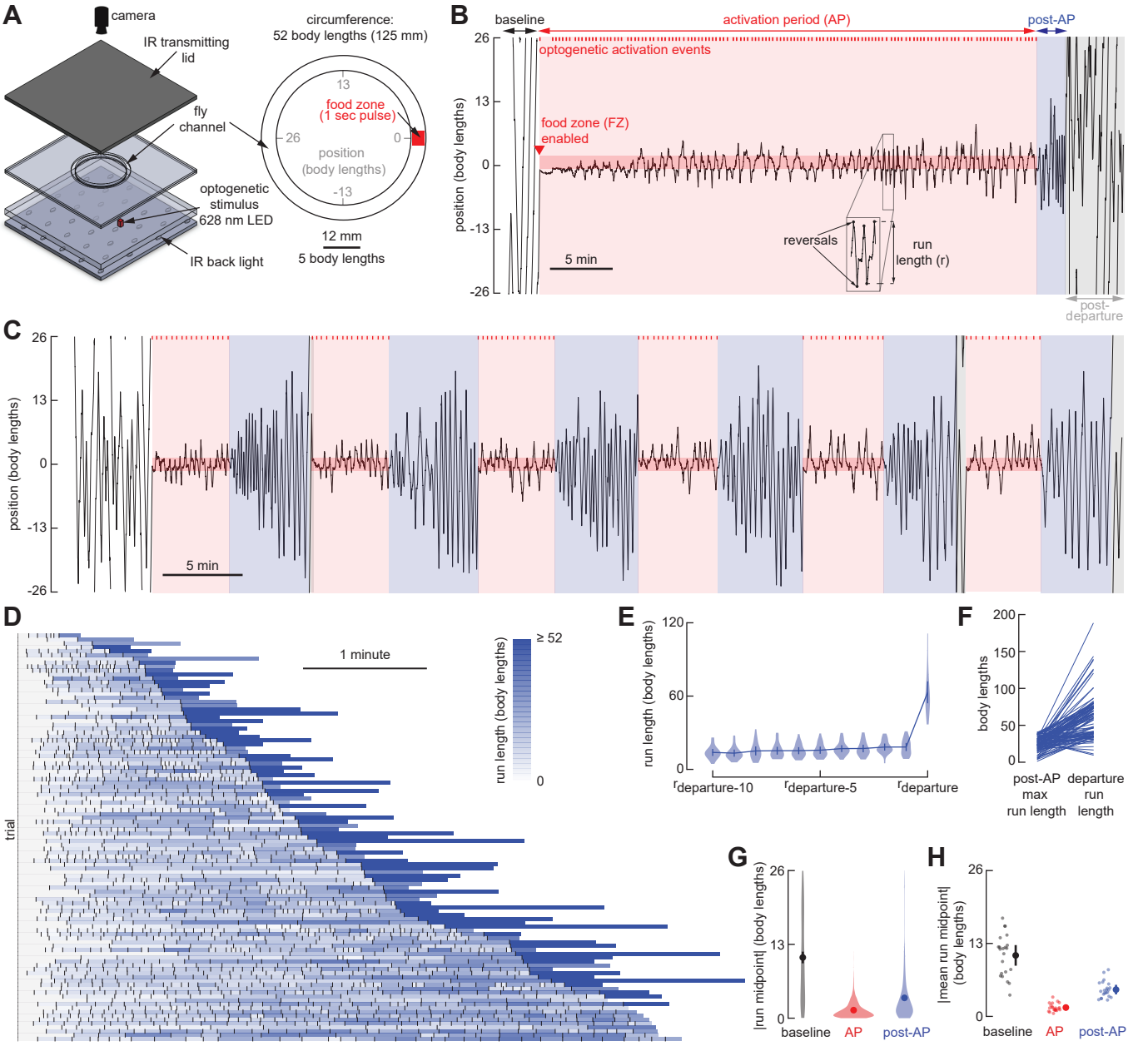

Figure 1. Repeated back-and-forth excursions constitute a local search around a fictive food location.

(A) Schematic of the experimental setup (left) and annular arena (right). An overhead camera tracks the position of an individual Gr5a-GAL4>UAS-CsChrimson female fly, in real-time, as it explores a 4 mm-wide circular channel, ~52 body lengths (BL) in circumference. Whenever the fly occupies the featureless food zone, it receives a one-second pulse of optogenetic activation of sugar-sensing neurons via a 628 nm LED positioned beneath the channel, followed by a 15-second refractory period during which the fly cannot receive activation. An infrared (IR) backlight and IR-transmitting lid enable behavioral tracking while otherwise maintaining complete darkness for the fly aside from the brief optogenetic pulses. (B) Example fly trajectory. To simplify the display and analysis of the data, we transformed the curved trajectories of the flies in the circular channel into a wrapped one-dimensional path. This experiment begins with a baseline period, during which the fly does not receive optogenetic activation, followed by a 40-minute activation period (AP, red) during which the optogenetic protocol is operational, followed by a post-activation-period (post-AP, blue) during which the optogenetic protocol is switched off. The post-AP is defined as ending when the fly executes its first run straying more than 26 body lengths (i.e., ½ the arena perimeter) from the food zone, hereafter termed the 'departure run'. The remaining trajectory is referred to as post-departure (grey). Optogenetic stimulation events during the AP are indicated as tick-marks (top). Inset: trajectories are analyzed to classify reversals of walking direction and run lengths (r)., i.e., the distance between consecutive reversals. (C) As in (B), for an experiment with six serial trials each consisting of a 5-minute AP followed by a 5-minute post-AP. (D) Sequences of post-AP runs, and their associated departure run, sorted by the duration of the post-AP. Each row corresponds to a single trial from experiments as in (C), where the length of each box corresponds to the duration of each run, and the color of each box indicates run length. (N = 22 flies, n = 110 trials). Note that in 11 trails at the bottom of the panel, the flies did not execute a departure run before the next AP began. (E) Run lengths for the final 10 runs of the post-AP, as well as the departure run, from data in (D). Data from trials with fewer than 10 post-AP runs are included. Throughout the paper, circles depict means, error bars depict 95% confidence intervals, and violin plots indicate full data distributions. (F) Length comparison of the longest post-AP run, and corresponding departure run, for each trial, from data in (D). The 11 trials without a departure run were not included in this analysis. (G) Distribution of the absolute value of the midpoint position of all runs from all trials from experiments as in (C), during baseline, AP, and post-AP. The 0 position indicates the center of the food zone. (N = 22 flies, n = 110 trials). Note, that because the data are expressed as absolute values, negative values are not permitted. (H) As in (G), showing the absolute value of the mean midpoint position of all runs from each fly. Grand means are plotted alongside individual datapoints.

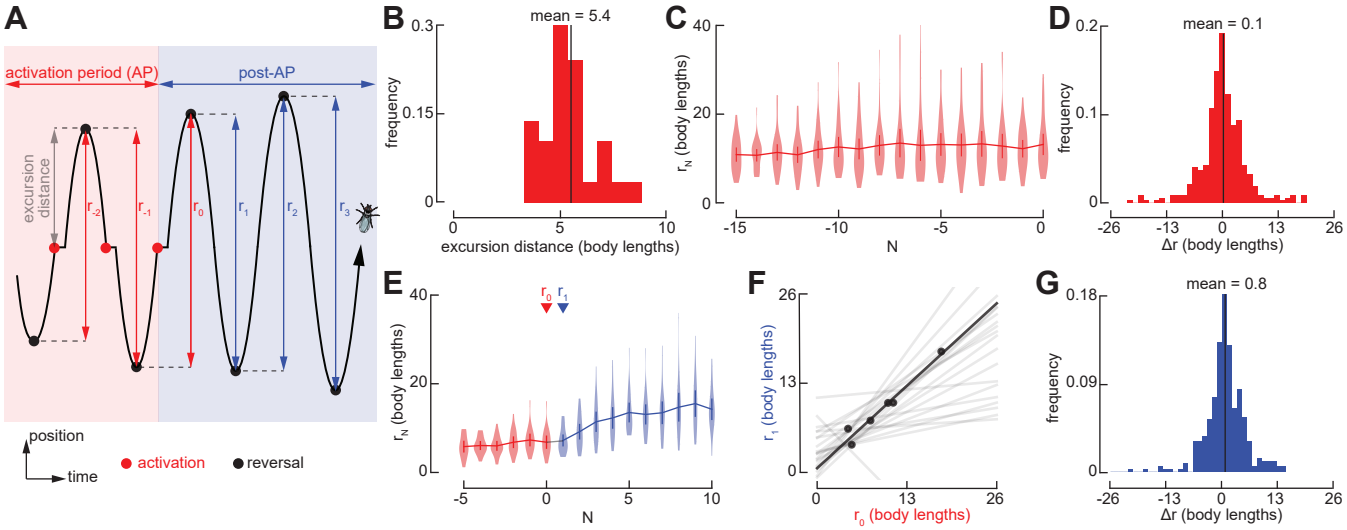

Figure 2. Local searches feature consistent run lengths.

(A) Schematic, showing features of local search. After encountering a food stimulus during the AP, flies walk a given excursion distance (grey), reverse direction, and perform a run back towards the food. The distance between two consecutive reversals is a run length (r), where r0 is the run length between the final reversal of the AP and the first reversal of the post-AP. (B) Mean distribution of excursion distances, from the 40-min AP experiments as in Figure 1B. (N = 29 flies). (C) Run lengths for the final 16 runs of the AP, including r0, from the 40-min AP experiments. Data from trials with fewer than 16 AP runs are included. (N = 29 flies). (D) Mean distribution of the difference in length between consecutive runs (Δr) during the AP, the 40-min AP experiments. (N = 29 flies). (E) Run lengths for the final 6 runs of the AP, including r0, and the first 10 runs of the post-AP, from the trial-based experiments as in Figure 1C. (N = 22 flies, n = 110 trials). Labels indicate the final run of the AP (r0) and the first run of the post-AP (r1). (F) Relationship between the final run of the AP (r0) and the first run of the post-AP (r1) from data in (E). Black dots indicate r0 vs. r1 for 6 trials from the fly in Figure 1C, and the black line indicates the linear regression for this fly. Grey lines indicate linear regressions for all remaining flies with data from at least 3 trials. (N = 20 flies). (G) Mean distribution of the difference in length between consecutive runs (Δr) during the first 10 runs of the post-AP, from data in (E).

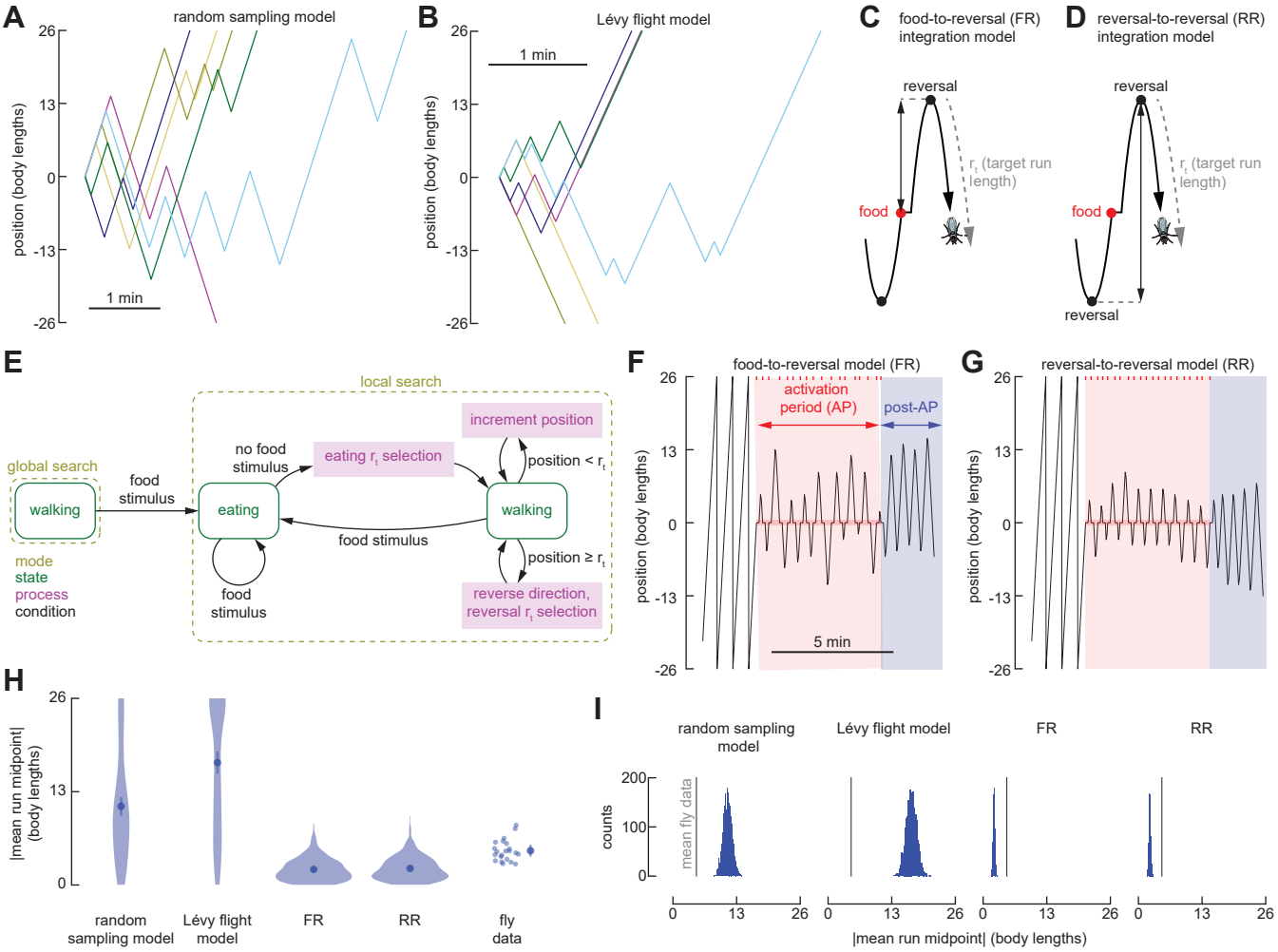

Figure 3. Agent-based models using iterative odometric integration recapitulate Drosophila local search.
(A) Six representative example trajectories from simulations for which run lengths were randomly drawn from the distribution of run lengths in Figure 1D (excluding the departure runs). Trajectories begin at the 0 position and are terminated when the simulated fly reaches 26 body lengths from the point of origin. (B) As in (A) from simulations for which run lengths were drawn from a Lévy flight distribution fit to the distribution of run lengths in Figure 1D (excluding the departure runs). (C) Schematic of food-to-reversal (FR) integration model. The fly keeps track of the distance walked between the location of a food stimulus and the subsequent reversal. This integrated distance influences the choice of target run length (rt) for the following run. (D) Schematic of reversal-to-reversal (RR) integration model. The fly keeps track of the distance walked between consecutive reversals. This integrated distance influences the choice of target run length (rt) for the following run. (E) Schematic of the state-transition diagram for FR and RR integration models. Arrows indicate transitions—governed by conditions—between search modes, behavioral states, and computational processes. For detailed state transition diagrams describing the FR and RR models, as well as the simulated environment, see Figure S1. (F) Example trajectory of FR model simulation, showing baseline, AP, and post-AP. Plotting conventions as in Figure 1B. (G) As in (F) for a RR model simulation. (H) Distribution of absolute value of mean post-AP midpoint position of all runs for agent-based models (n = 300 simulations as in (F) and (G)). For comparison, fly data are replotted from Figure 1H. (I) Statistical comparison of agent-based models and fly data. Histograms show distributions of the absolute value of mean run midpoint position, calculated from 2,000 random samples from distributions in (H). Vertical lines indicate the grand mean run midpoint of fly data in (H).

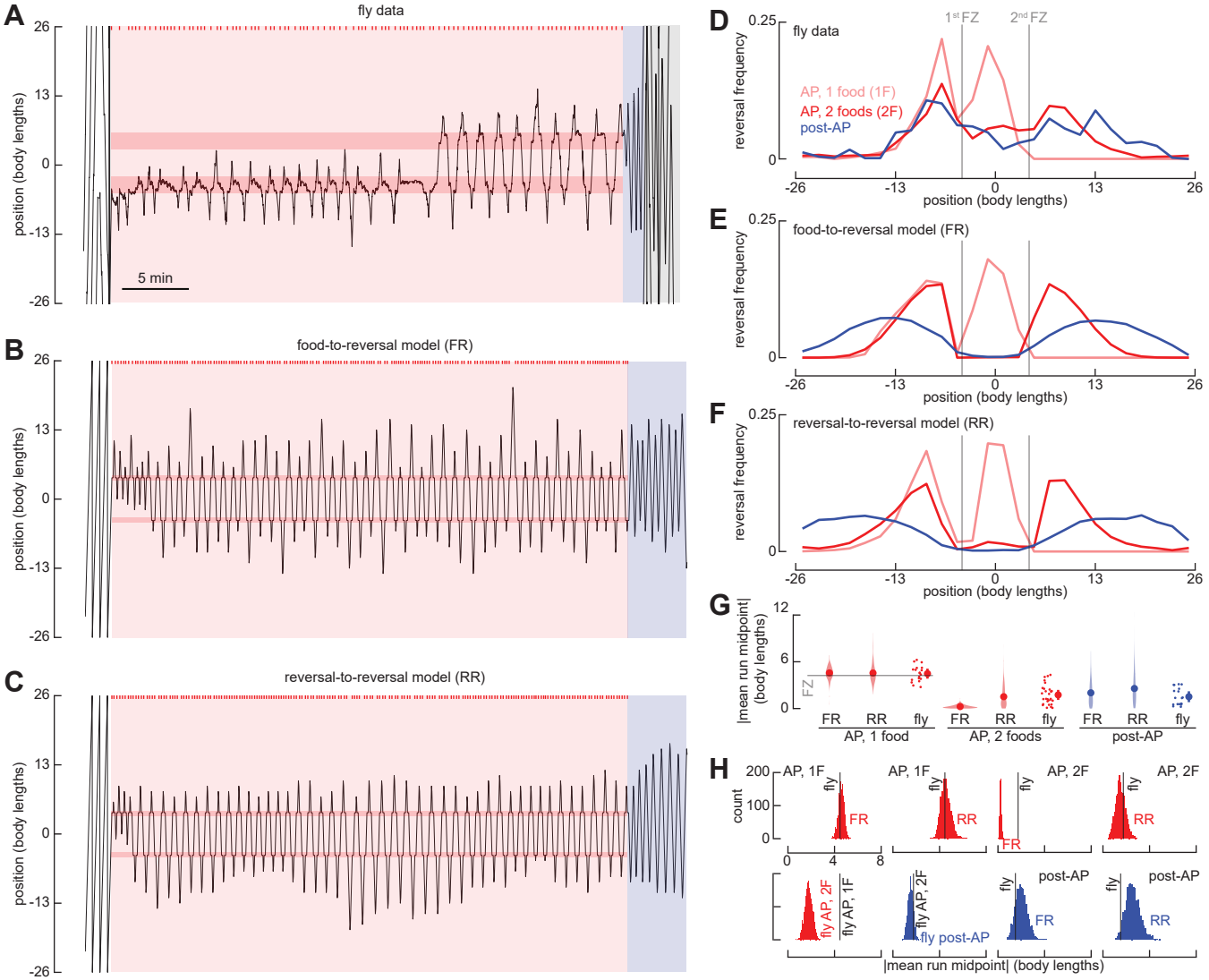

Figure 4. Iterative odometric integration enables local search around multiple fictive food sites.
(A) Example trajectory of a fly exploring an annular arena with two food zones, spaced 9 body lengths (BL) apart. The experiment consists of a baseline period, AP, and post-AP. Plotting conventions as in Figure 1B. (B) As in (A), for a simulation using the FR model. (C) As in (A), for a simulation using the RR model. (D) Mean distribution of reversal locations during fly experiments as in (A). Histograms were calculated using 2 BL bins. Distributions are plotted for the one-food search (1F, light red), the two-food search (trajectory after the fly has encountered the 2nd food zone, 2F, dark red), and the post-AP (blue). To align data for analysis, distributions from some experiments were inverted such that the location of the 1st food zone is always at the 4.5 BL position. For each experiment, 1F, 2F, or post-AP distributions consisting of fewer than 5 total reversals were discarded from this analysis. (N = 29 flies). (E) As in (D) for simulations using the FR model. (F) As in (D) for simulations using the RR model. (G) Distribution of absolute value of mean midpoint position of all runs for odometric integration models (n = 300 simulations), as well as from each fly, from data in (D-F). Grand mean of the absolute value of run midpoint positions is plotted alongside fly data. (H) Statistical comparisons of run midpoints of odometric integration models and fly data during experiments with multiple food zones. Histograms show the distribution of the absolute value of mean run midpoint position for the indicated dataset and experimental period, calculated from 2,000 random samples from distributions in (G). Vertical lines indicate mean or grand mean of indicated dataset or experimental period from data in (G).

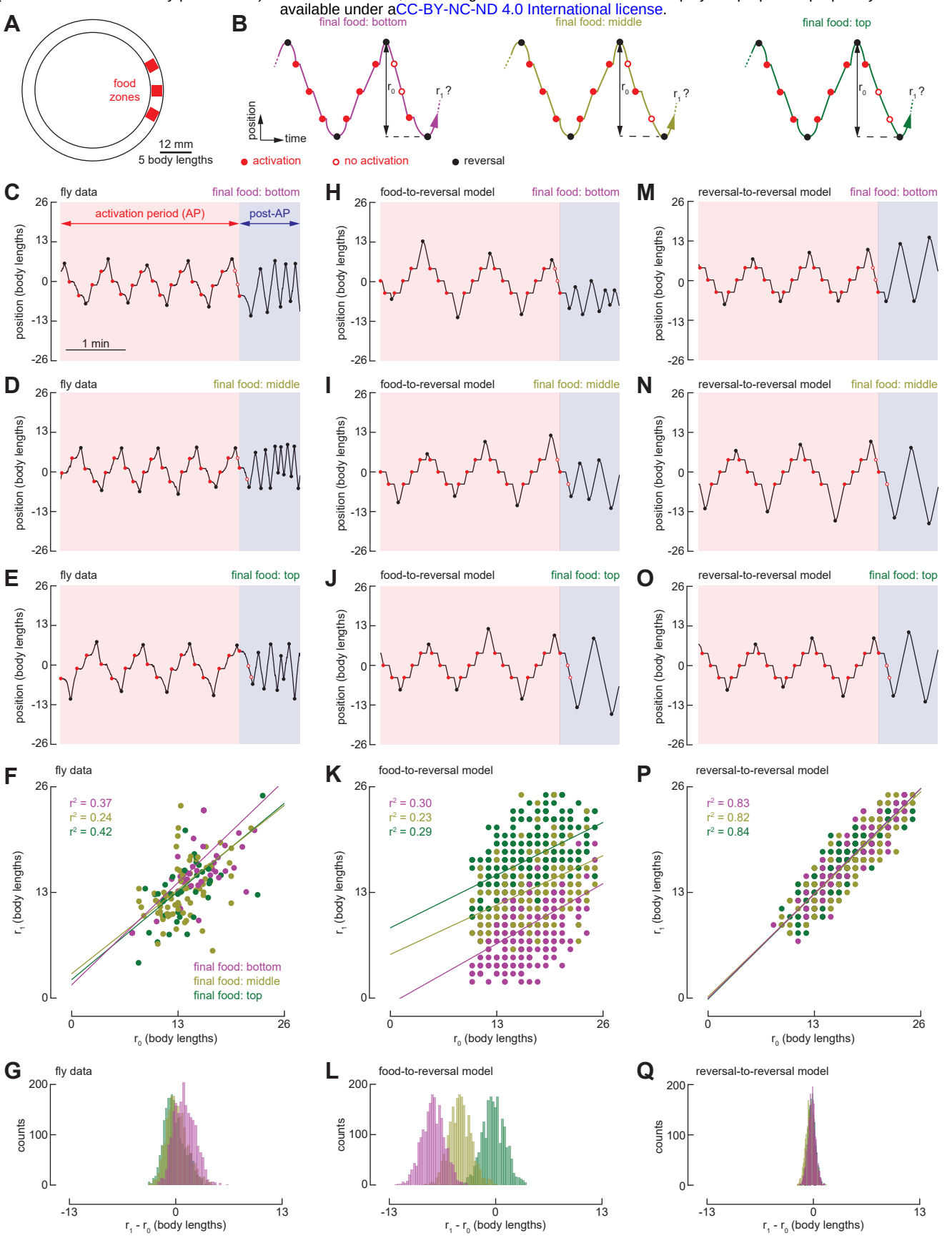

Figure 5. Flies center local search around multiple fictive food sites by integrating the distance walked between consecutive reversals.
(A) Schematic of the annular arena with three food zones, spaced 4.5 body lengths apart. (B) Schematic of the experimental paradigm. At the conclusion of the AP, two of the food zones were disabled while one food zone remained capable of providing an additional single optogenetic pulse. For each trial, the final operational food zone was designated to be either the bottom, middle, or top. For trials where the final 3 or more runs during the AP spanned all three food zones, we compared r0 and r1, where r0 is the run length between the final reversal of the AP and the first reversal following the final food stimulus. (C-E) Example trajectories of a fly searching across three food zones, in which the final food stimulus is in either the bottom (C), middle (D), or top (E) position. (F) Relationship between r0 and r1 for three-food experiments with flies, in which the final food stimulus is in either the bottom, middle, or top position. Lines and r2 values indicate linear regressions for the three conditions. (N = 45 flies, n = 166 trials). (G) Statistical comparisons of run lengths in three-food experiments where the final food stimulus is in either the bottom, middle, or top position. Histograms show distributions of the mean difference between r1 and r0, calculated from 2,000 random samples of the mean of 10 points from distributions in (F). (H-L) As in (C-G), for simulations using the FR model. (n = 300 simulations). (M-Q) As in (C-G), for simulations using the RR model. (n = 300 simulations).

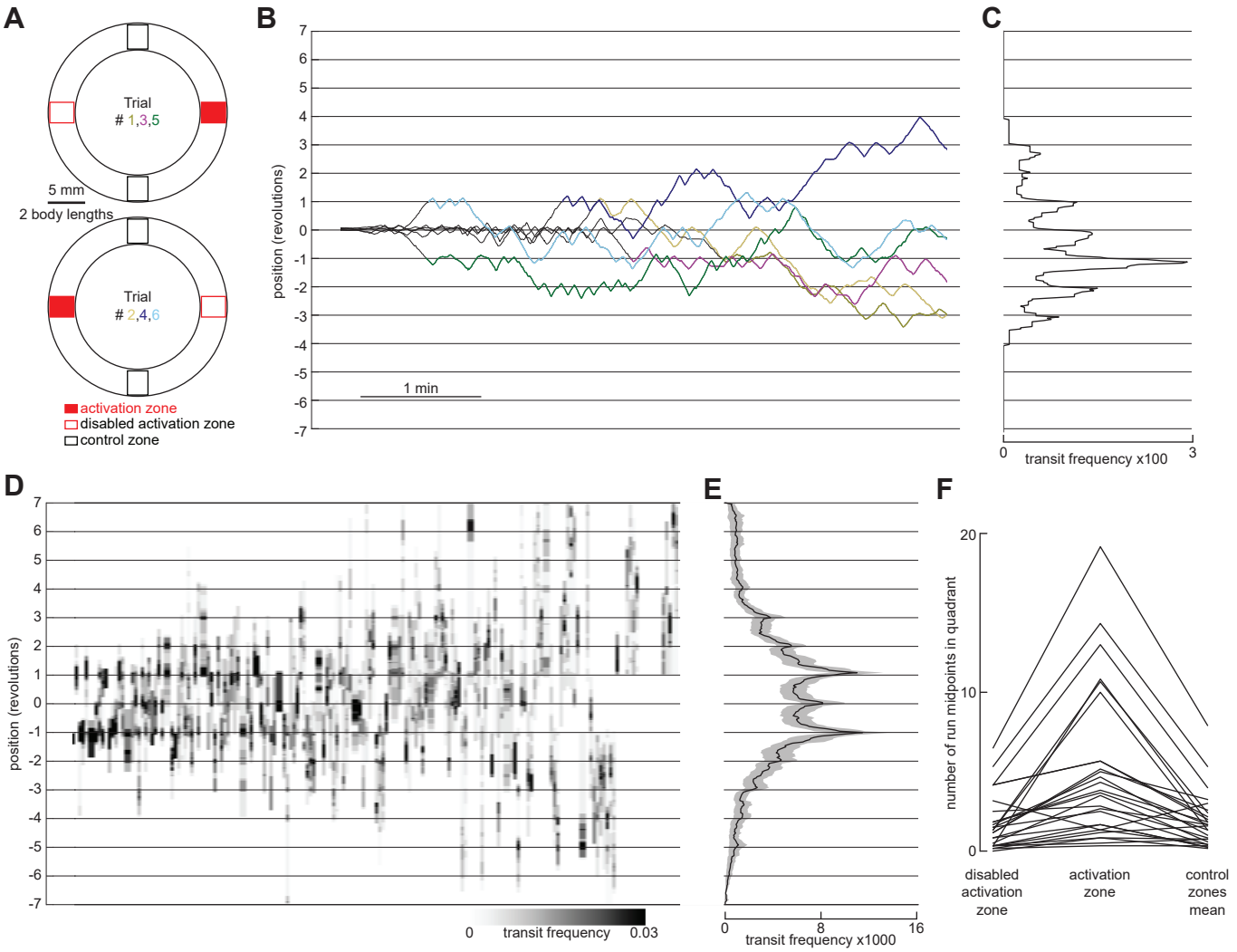

Figure 6. Flies reinitiate a local search at a former fictive food site after circling the arena.

(A) Schematic of the smaller annular arena (~26 body lengths), indicating the location of the food zone for each trial, as well as control zones used for analysis. Experiments were done as in Figure 1C, but each food zone was 1.3 body lengths, and the food zone location was alternated from trial to trial. (B) Example post-AP (grey) and post-departure (colored) trajectories from a single experiment where each line corresponds to a single trial and shows the unwrapped trajectory, with gridlines indicating full revolutions around the arena. To align data for analysis, trajectories from even-numbered trials were shifted such that the location of the food zone is always at 0. (C) Mean distribution of fly transits for post-departure trajectories in (B). Transits were calculated using bins 2 BL wide and counted when a fly entered a bin from one side and exited the bin from the other side. (D) Heatmap indicating distribution of transits during post-departure trajectories, calculated using 4 bins per revolution (dividing the arena into quadrants centered on the food zone, disabled food zone, and control zones). Each column represents a single trial, with columns sorted by frequency of transits at the 1 or -1 revolution position. (N = 28 flies, n = 168 trials). (E) Mean transit distribution for data in (D). Shaded grey region indicates 95% confidence interval. (F) Number of run midpoints in each arena quadrant during post-departure trajectories. Each line shows the mean values for a single fly, where data from both control quadrants were averaged together.

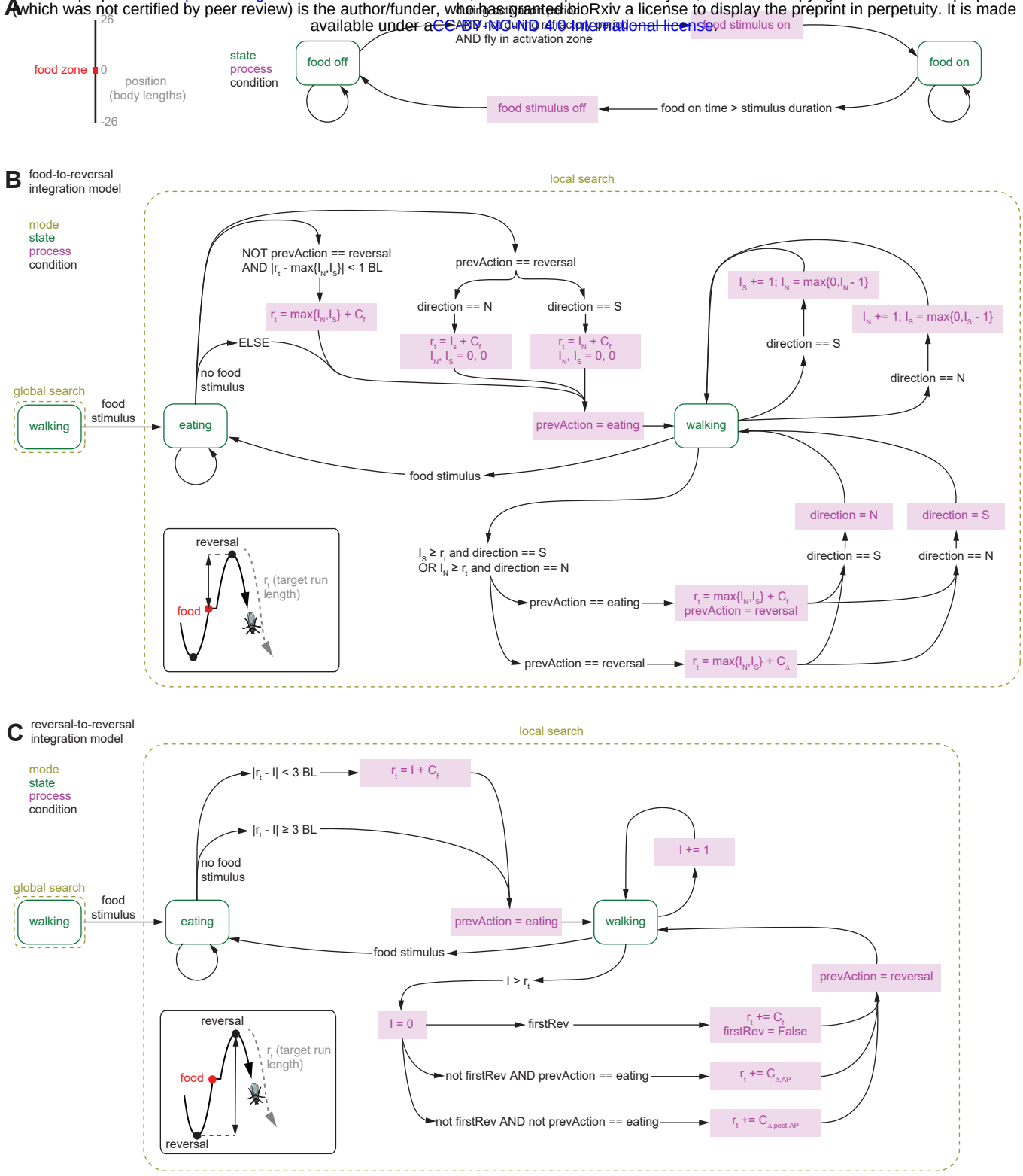

Supplementary Figure 1. State-transition diagrams describing agent-based odometric integration models of Drosophila local search, related to Figure 3.

(A) Left: Schematic of the simulated 1-dimensional environment. The example shown here is for a simulated environment with a single food zone. Right: State transition diagram for the simulated environment. The simulated environment is in either the food on or off state. Transitions between these states, via processes, are determined by the conditions at each timestep of the simulation. See methods for details. (B-C) State transition diagrams for the food-to-reversal (FR) integration model (B) and the reversal-to-reversal (RR) integration model (C). The simulated fly can either be in an eating or walking state, within either a global or local search mode. Transitions between these states and modes, sometimes via processes, are determined by the conditions at each timestep of the simulation. (rt = target run length, BL = body lengths, I = Integrator, N = North, S = South, prevAction = previous action, firstRev = first reversal). The variables Cf, CΔ, CΔ,AP, and CΔ,post-AP, represent a value drawn from the corresponding distribution. See methods for details.

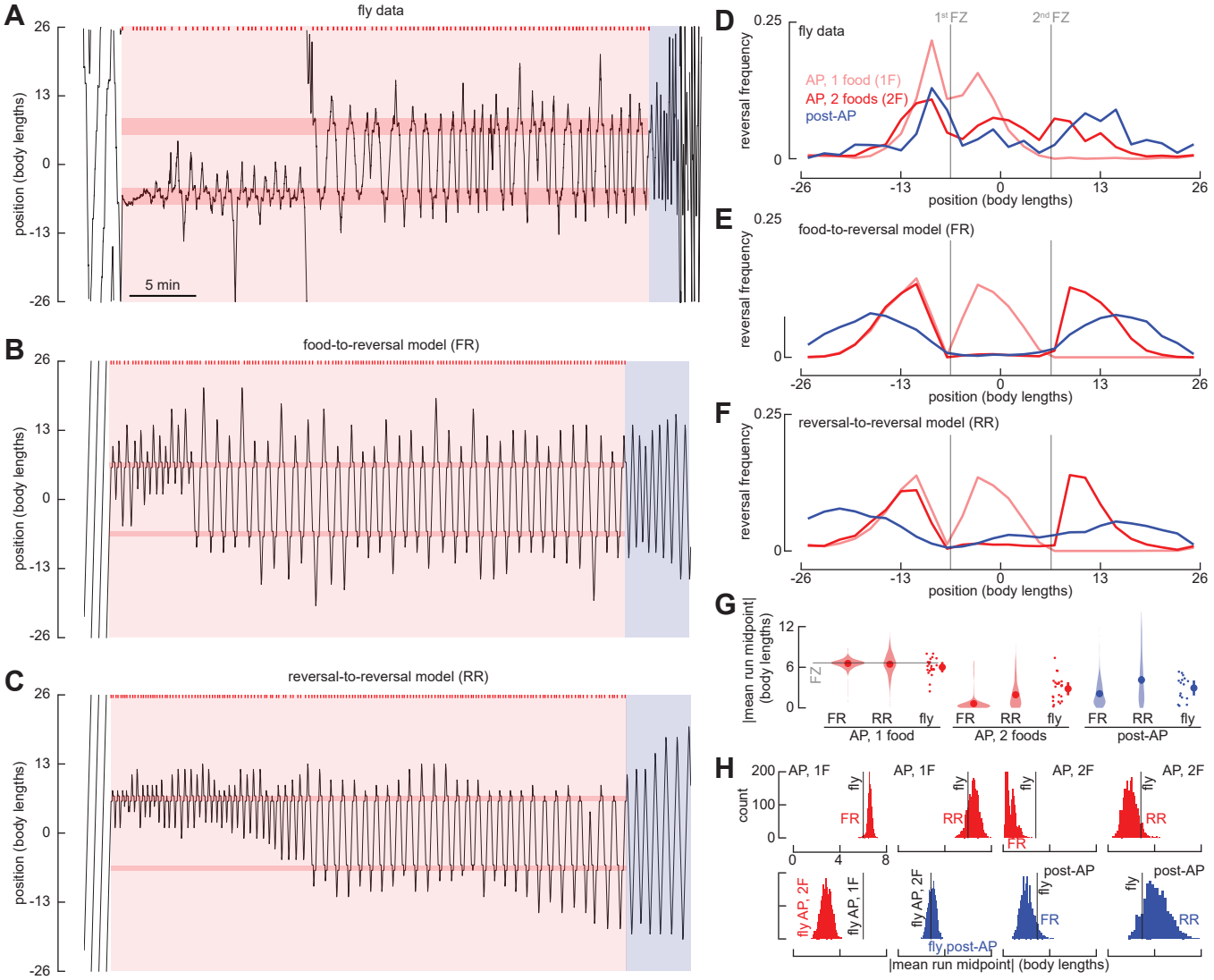

Supplementary Figure 2. Iterative odometric integration enables local search around fictive food sites spaced 13 body lengths apart, related to Figure 4

(A-I) As in Figure 4, for experiments where the food zones are located 13 body lengths apart. (N = 27 flies).

.

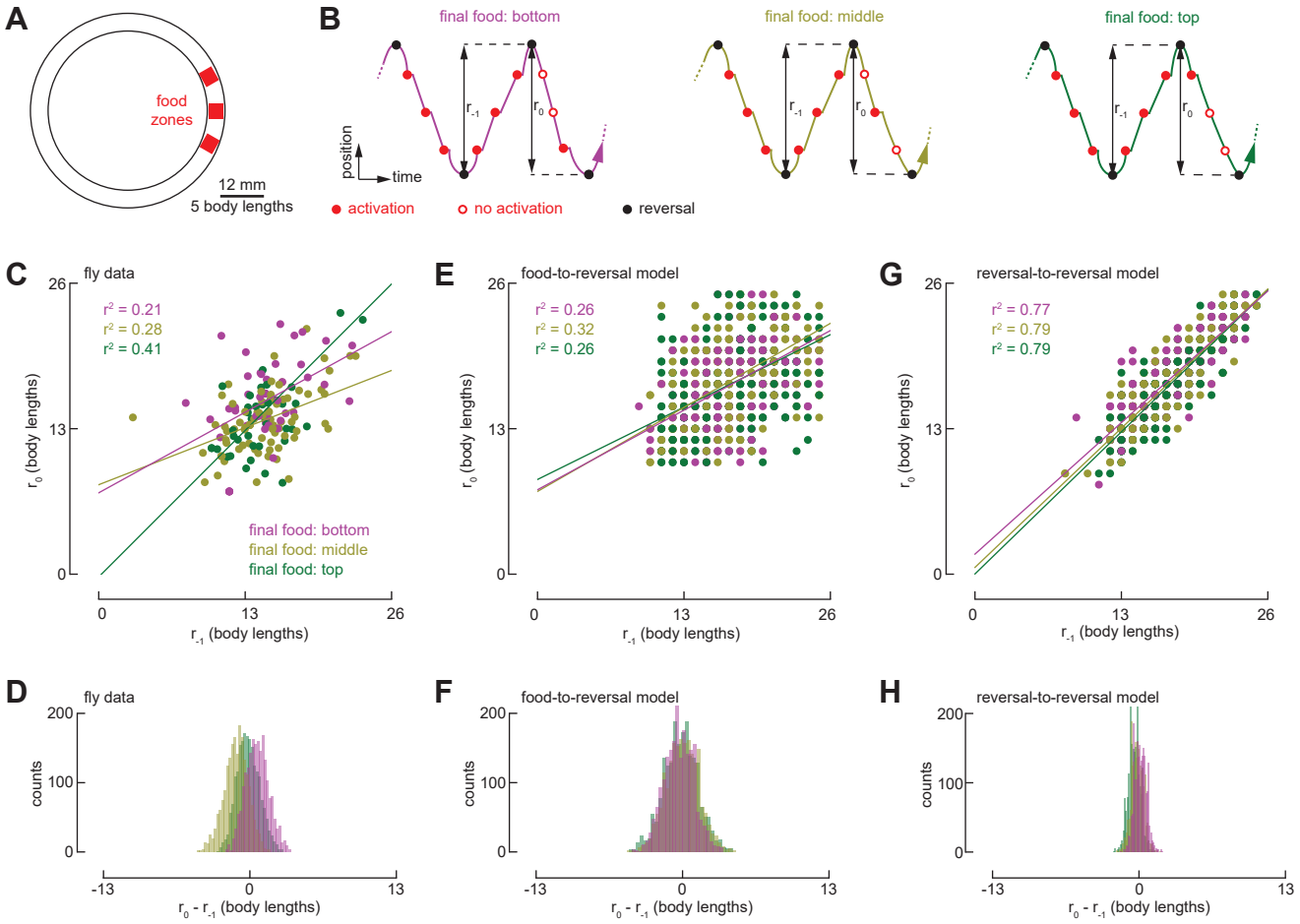

Supplementary Figure 3. Flies and odometric integration models maintain constant run lengths during the AP, related to Figure 6

(A) Schematic of the annular arena with three food zones, spaced 4.5 BL apart. (B) Schematic of experimental conditions. At the conclusion of the AP, two of the food zones were disabled, while one food zone remained temporarily operational, capable of providing an additional single optogenetic pulse. For each trial, the final operational food zone was randomly designated to be either the bottom, middle, or top food zone. For trials where at least the final 3 or more runs during the AP spanned all three food zones, we analyzed the distance between the final two reversals during the AP (r0) as well as the distance between the penultimate reversal of the AP and the preceding reversal (r-1). (C) Relationship between r0 and r-1 for three-food experiments with flies, where the final food stimulus is in either the bottom, middle, or top position. Lines and r2 values indicate linear regressions for the three conditions. (N = 45 flies, n = 166 trials). (D) Statistical comparisons of run lengths in three-food experiments where the final food stimulus is in either the bottom, middle, or top position. Histograms show distributions of the mean difference between r-1 and r0, calculated from the means of 2000 random samples of 10 points from the distributions in (C). (E-F) As in (C-D), for simulations using the FR model. (n = 300 simulations per condition). (G-H) As in (C-D), for simulations using the RR model. (n = 300 simulations per condition).

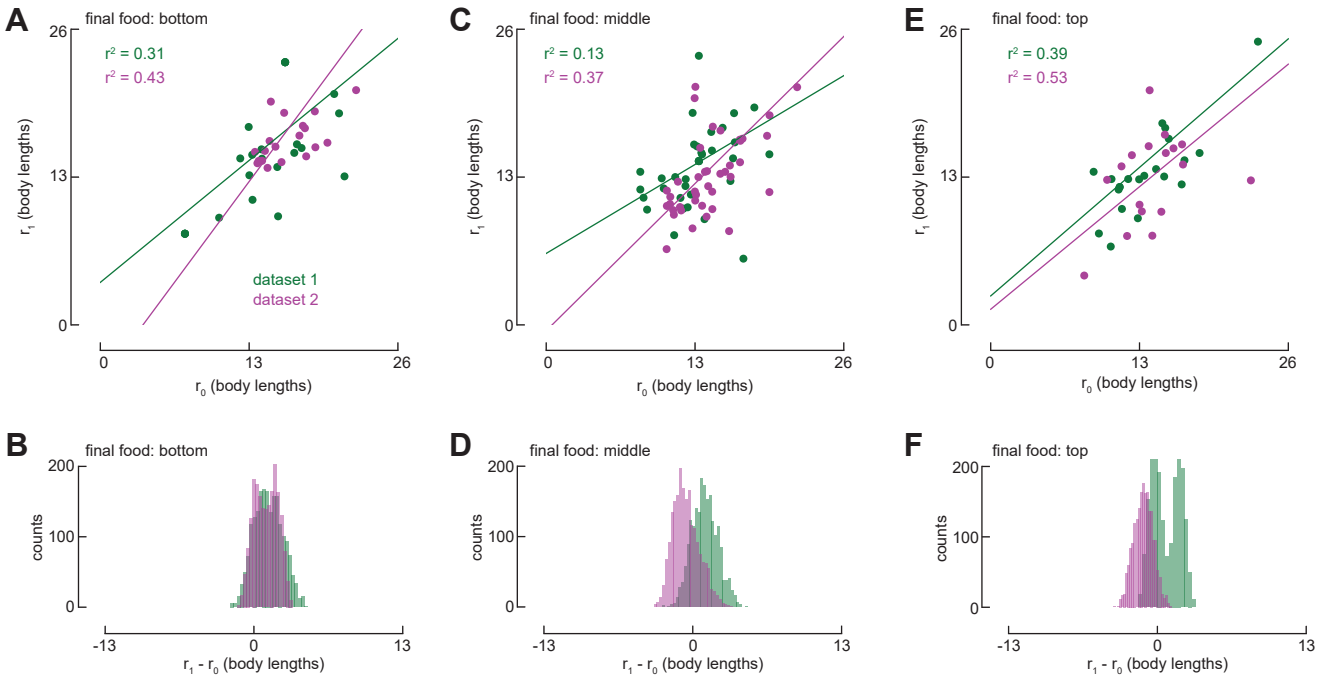

Supplementary Figure 4. Results from 3-food paradigm were highly consistent across experiments performed many months apart, related to Figure 6

(A) Relationship between r0 and r1 for three-food experiments conducted in March 2020 (dataset 1, green, N = 23 flies, n = 78 trials) or September 2020 (dataset 2, purple, N = 22 flies, n = 88 trials), for trials where the final food stimulus is in the bottom position. Lines and r2 values indicate linear regressions for the two datasets. These datasets are combined in Figure 6. (B) Statistical comparisons of three-food experiment datasets. Histograms show distributions of the mean difference between r1 and r0, calculated from the means of 2000 random samples of 10 points from the distributions in (A). (C-D) As in (A-B), for trials where the final food stimulus is in the middle position. (E- F) As in (A-B), for trials where the final food stimulus is in the top position.